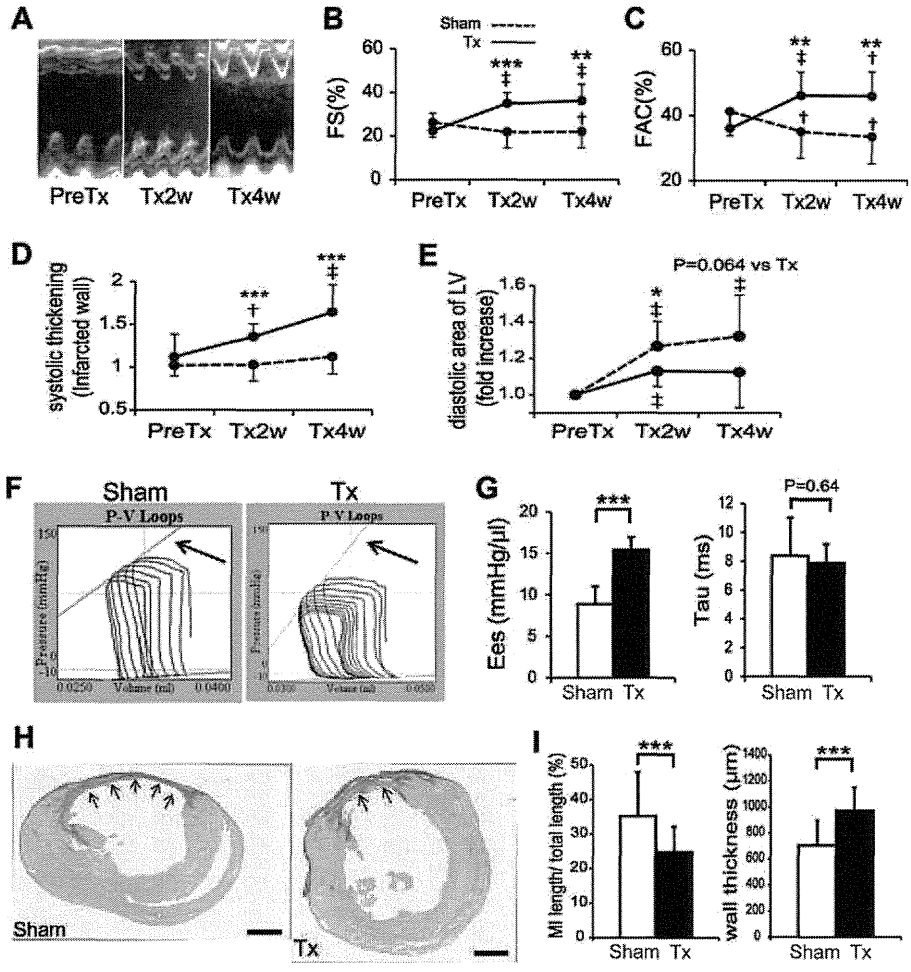

Figure 2. Cardiac functions after cardiac tissue transplantation to rat MI. (A–F): Echocardiogram ($n = 9$). (A): Representative M-mode image. Note that infarct anterior wall started to move 2–4 weeks after transplantation (Tx). (B): FS. (C): FAC. (D): Systolic thickening of infarcted wall. (E): Diastolic area of LV (fold increase to PreTx). (F, G): LV pressure-volume (P-V) loop study 4 weeks after Tx ($n = 8$). (F): Representative P-V loops. Slopes indicate Ees (arrows). (G): Ees: End-systolic elastance (left panel). Tau: time constant (right panel). (H, I): Sirius red staining at Tx4w. (H): Representative sections. Reduction of fibrotic area and wall thinning after Tx indicates attenuation of LV remodeling (arrows). (I): The ratio of MI length of total length (left panel) and wall thickness of infarct wall (average thickness) (right panel) (25 sections). *, $p < .05$; **, $p < .01$; and ***, $p < .001$ (unpaired t test). †, $p < .05$ and ‡, $p < .01$ (vs. PreTx, paired t test). PreTx, Pretransplantation; Tx2w, Tx4w, 2 and 4 weeks after transplantation, respectively. Scale bars = 1 mm. Abbreviations: FAC, fractional area change; FS, fractional shortening; LV, left ventricle; MI, myocardial infarction.

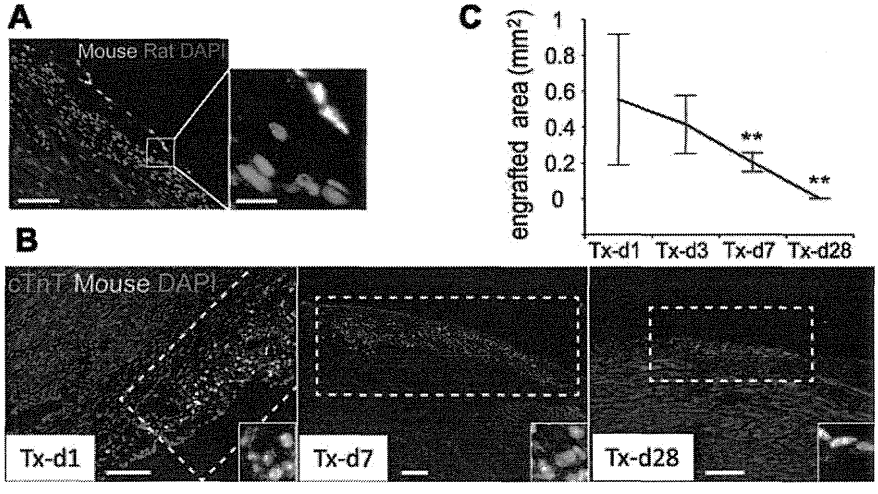

Figure 3. Tracing of transplanted cells with species-specific fluorescent in situ hybridization (SS-FISH). (**A**): SS-FISH analysis for mouse (yellow) and rat nuclei (magenta). Just after transplantation of mouse monolayer cell sheet. Right panel: higher magnification view of boxed area. (**B**, **C**): Cell tracing after transplantation. (B): Double staining for cTnT (immunostaining, red), SS-FISH (mouse nuclei, yellow), and DAPI. Dotted squares indicate engrafted clusters. Insets: higher magnification views. (C): Quantification of engrafted area (mouse nuclei^{+}/cTnT^{+} area [mm^2], $n = 10$): 0.55 ± 0.36 (Tx-d1), 0.42 ± 0.16 (Tx-d3), 0.20 ± 0.05 (Tx-d7), and 0.0023 ± 0.0008 (Tx-d28). **, $p < .01$ (vs. Tx-d1, unpaired t test). Tx-d1, d3, d7, and d28: 1, 3, 7, and 28 days after Tx, respectively. Scale bars = 100 μm in (A) (left panel), 20 μm in (A) (right panel), and 200 μm in (B). Abbreviations: cTnT, cardiac troponin-T; DAPI, 4,6-diamidino-2-phenylindole.

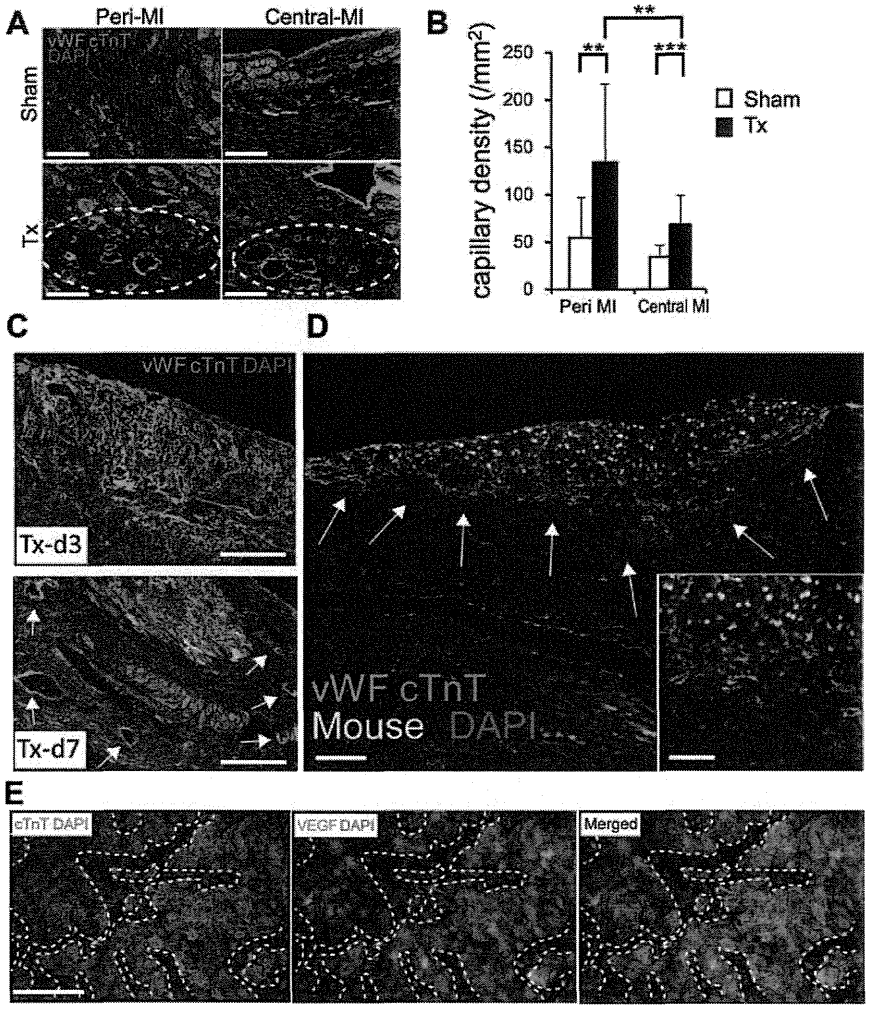

Figure 4. Neovascularization after transplantation. (**A**, **B**): Capillary formation at Tx-d28. (A): Double staining for vWF (ECs, green) and cTnT (cardiomyocytes [CMs], red) at peri-MI and central-MI areas (Supporting Information Fig. S4A). Note that newly formed capillaries are clearly observed in transplantation group (dotted circles). (B): Quantification of capillary density (capillary number per square millimeter). Peri-MI area (left panel) and central-MI area (right panel) (15 views each). **, $p < .01$ and ***, $p < .001$ between corresponding values (unpaired t test). (**C**, **D**): Kinetics (C) and origin (D) of neovascularization. (C): Double staining for vWF (green), cTnT (red), and DAPI. Note that prominent vWF^+ cell accumulation in the proximity of grafted CMs (Tx-d3, upper panel) and induction of vascular structures with lumen are observed (arrows, Tx-d7, lower panel). (D): Triple staining for vWF, cTnT, and species-specific fluorescent in situ hybridization (mouse nuclei, yellow) (Tx-d3). Most of the accumulated vWF^+ cells are negative for mouse nuclear staining (arrows). Inset: higher magnification view. (**E**): Double staining for VEGF (green) and cTnT in tissue sheet in vitro. VEGF expression is restricted to $cTnT^+$ area. Dotted lines: boundary of cTnT-positive and negative area. Scale bars = 100 μm in (A, C, D) (main panel) and (E) (left panel), 50 μm in (D) (inset). Abbreviations: cTnT, cardiac troponin-T; DAPI, 4,6-diamidino-2-phenylindole; MI, myocardial infarction; VEGF, vascular endothelial cell growth factor; vWF, von Willebrand factor.

paracrine effects, of the sheet at the early stage of transplantation.

Neovascularization Following Cardiac Tissue Sheet Transplantation

Neovascularization is one of the major phenomena in paracrine effects reported in BM cell transplantation [25]. We examined neovascularization after cardiac tissue transplantation with von Willebrand factor (vWF) staining for ECs and found that capillary density was significantly increased within both peri-MI and central-MI (more prominent in peri-MI) area 4 weeks after transplantation (Fig. 4A, 4B) (peri- and central-MI are illustrated on Supporting Information Fig. S4A). We further examined the kinetics and cellular origin of the neovascularization. One day after transplantation, vWF^+ cells were distributed within the engrafted area but not evident outside of this area (data not shown). At 3 days after transplantation, prominent accumulation of vWF^+ cells was observed in the proximity of the engrafted area (Fig. 4C; Supporting Information Fig. S4B). SS-FISH revealed that the accumulated cells originated from the recipients but not from the grafts (Fig. 4D). At 7 days after transplantation, capillaries with lumen that originated from the recipients were generated in the area around the graft (Fig. 4C). These results indicate that cardiac tissue sheet transplantation potently induces the accumulation of endogenous vascular cells and capillary formation around the engrafted sheet within the early stages of transplantation.

Next, to elucidate the molecular mechanism of the neovascularization, we examined protein secretion of some angiogenic factors such as tumor necrosis factor-alpha, insulin-like growth factor 1, VEGF, interleukin-6, basic fibroblast growth

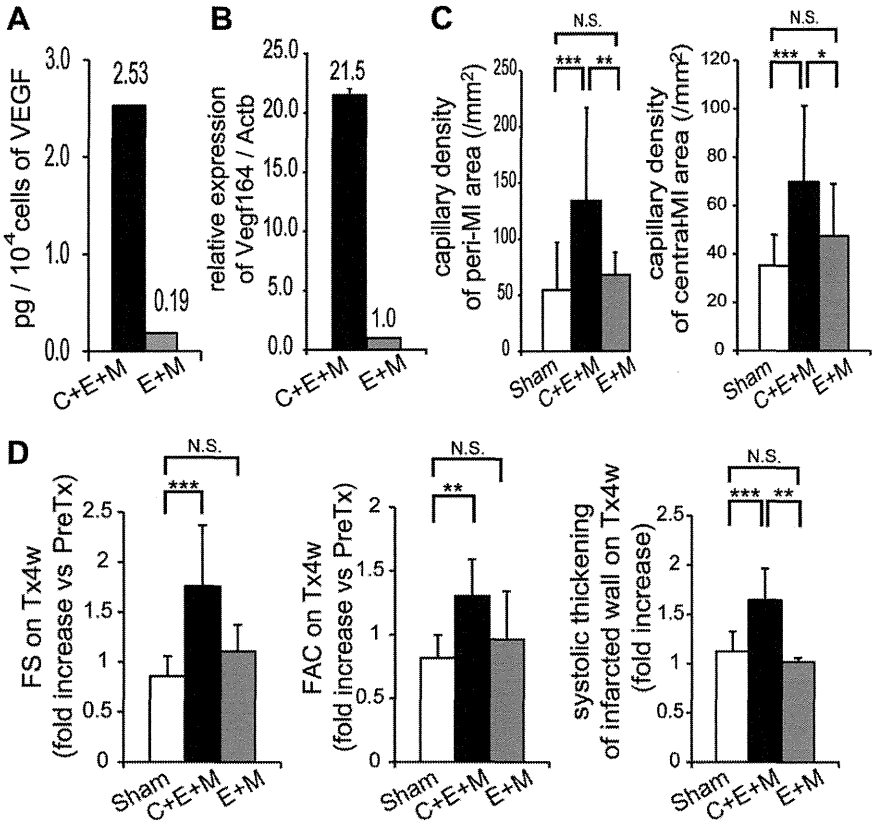

Figure 5. Cell type-controlled sheet analyses. (**A**): ELISA for VEGF secretion (picogram per10^4 cells) in culture supernatants of C + E + M and E + M sheets. (**B**): Quantitative PCR for VEGF mRNA from C + E + M and E + M sheets. Vegf164 (VEGF) expressions were normalized by Actb (β-actin) expression. Expressions in E + M sheets were set as 1.0. (**C, D**): Transplantation of sham operation ($n = 9$) versus C + E + M sheets ($n = 9$) versus E + M sheets ($n = 3$) (Tx-d28). (C): Capillary density (capillary number per square millimeter). Peri-MI area (left panel) and central-MI area (right panel) (15 views each). (D): Echocardiogram data (fold increase vs. PreTx). FS (left panel), FAC (middle panel), and systolic thickening of infarct wall (right panel). *, $p < .05$; **, $p < .01$; and ***, $p < .001$ (unpaired t test). C: *C*Ms, E: *E*Cs, M: *M*Cs. Abbreviations: FAC, fractional area change; FS, fractional shortening; MI, myocardial infarction; N.S., not significant; VEGF, vascular endothelial cell growth factor.

factor (bFGF), interferon-gamma, epidermal growth factor, leptin, and hepatocyte growth factor in the culture supernatant of cardiac tissue sheet. Among them, VEGF production was much more prominent than the other factors, suggesting the critical role of VEGF (Supporting Information Fig. S4C). To identify the cell populations responsible for VEGF production, we performed immunofluorescent staining of cardiac tissue sheet. VEGF staining was highly restricted to $cTnT^+$ CM area (Fig. 4E), indicating that CMs are the main source of VEGF among sheet-composing cell types.

Prospective Examination of Functional Roles of CMs with Cell Type-Controlled Tissue Sheets

Our ESC system possesses distinct advantages from previous cell transplantation studies, in which we can prospectively evaluate the functional roles of each cell population by cell type-controlled sheets with various combinations of cardiovascular cells. VEGF secretion from C + E + M sheet in vitro was 13.3-fold higher (Fig. 5A), and Vegf164 gene expression in vitro was 21.5-fold higher (Fig. 5B) than those from E + M sheet (*E*Cs and *M*Cs) (Supporting Information Fig. S5A), respectively. These results confirm the result of immunostaining for VEGF (Fig. 4E). Next, we performed transplantation of E + M sheets (three-layered) and compared the capillary densities and cardiac functions to those of C + E + M sheet transplantation group. Transplantation of E + M sheets did not induce significant increase in capillary density (Fig. 5C). Echocardiogram revealed that the improvement of systolic function was diminished in E + M sheet transplantation (Fig. 5D). These results indicate that sheet CMs are essential to achieve cardiac functional improvement in the infarct heart.

Roles of ECs and MCs in Cardiac Tissue Sheet Transplantation

Cellular interactions among CMs and nonmyocytes are considered to be involved in myocardial tissue formation and function [44, 45]. Coculture of neonatal rat ECs and CMs is reported to enhance secretion of angiogenic factors such as VEGF [35]. To estimate the role of ECs in the cardiac tissue sheet function, we generated sheets with *C*Ms and *M*Cs (C + M sheet) without ECs and examined the effect of ECs on VEGF secretion (Supporting Information Fig. S5B). CMs in C + M sheet showed a significantly lower positive rate of VEGF (Supporting Information Fig. S5C, S5D) and VEGF secretion in culture supernatant (0.33-fold increase), compared with those in C + E + M sheet (Supporting Information Fig. S5E), indicating that existence of ECs in the tissue sheets promotes VEGF production from CMs.

We also found significant roles of MCs through trying to generate cell sheet without MCs. When various amounts of purified CMs were plated onto the 12-multiwell UpCell (2.5×10^5, 5.0×10^5, or 1.0×10^6 per well) to form pure CM sheet without MCs, pure CMs failed to form sheet structure regardless of the plated cell counts. Sheet formation was

successfully recovered by plating the mixture of CMs and MCs onto UpCell dishes (Supporting Information Fig. S5F), suggesting that MCs are essential to form an integrative cell sheet structure. These results indicate that ECs and MCs play critical and beneficial roles in cardiac tissue sheet formation and function through cellular interaction.

Discussion

In this study, we showed therapeutic potential of cardiac tissue sheets from pluripotent stem cells and novel cellular mechanisms of cardiac functional improvement with a prospective strategy by reassembling defined cardiac cell populations (Supporting Information Fig. S6). Cardiac tissue sheet transplantation distinctively restored cardiac function after MI mainly through the suppression of LV remodeling with the induction of neovascularization in the proximity of the sheet. CMs played a central role for the functional restoration not through direct contribution but through the induction of neovascularization. Cellular interaction among CMs, ECs, and MCs efficiently enhanced structural integration and function of the cell sheets. Understanding the roles of each transplanted cell population, especially the new role of CMs, would provide a valuable strategic principle in future therapy for cardiac restoration.

In this study, we used SS-FISH, which can distinctively stain and discriminate mouse and rat nuclei. This method is amenable to sensitive and specific tracing of transplanted mouse ESC derivatives, avoiding the problem of transgene silencing during ESC differentiation, and false positives of transplanted cell marking by cell fusion phenomena [42, 43]. The results clearly showed that even though apparent improvement of cardiac function was induced and sustained long after transplantation, the majority of the grafted cells diminished within the earlier period. Moreover, massive neovascularization originating from the recipients was induced in the proximity of the transplanted sheets, indicating that graft-elicited neovascularization is critical for suppression of LV remodeling and following functional restoration. LV remodeling is a complex alteration in ventricular architecture after MI. During scar formation and tensile strength increase, the infarct region becomes thinner and elongates due to continuous expansive stimulation, termed "infarct expansion" (Supporting Information Video 4) [46–48]. Infarct expansion finally results in LV remodeling with dilated LV lumen and fibrous tissue deposition. It is also said that the viable myocardium in the infarct border zone is significantly hypertrophied following infarction. The impaired capillary network that cannot support the demand of hypertrophied myocardium accelerates infarct expansion [46]. Thus, a sufficient blood supply to the border zones is critical to prevent infarct expansion. Indeed, induction of neovascularization by BM-derived cell transplantation to MI model was reported to attenuate infarct expansion and LV remodeling [25]. Predominant neovascularization in border zone following cardiac tissue sheet transplantation should contribute to suppress infarct expansion and LV remodeling through attenuation of capillary insufficiency.

Some previous studies with stem cell transplantation, including cell sheet experiments (stem cell antigen 1-positive cardiac progenitor cells or adipose tissue-derived mesenchymal stem cells), showed functional restoration after MI [6, 9, 19–21, 23, 25, 36]. Nevertheless, their precise cellular mechanisms still remain unclear [26, 27] possibly because of the heterogeneity of the consisting cell populations of the sheet with various lineages or differentiation stages. How can we achieve a more profound elucidation of the mechanism, which is hampered due to the heterogeneity of the transplanted cells? Recently, Yoon et al. tackled this issue through the injection of genetically modified lines of BM mononuclear cells for acute MI model, followed by selective cell depletions of CMs (αMHC^{+}), ECs (endothelial nitric oxide synthase positive), or MCs ($SM22\alpha^{+}$) 2 weeks after injection [49]. The results that elimination of ECs or MCs induced a significant deterioration of cardiac function suggested the importance of angiogenesis in functional restoration after BM cell therapy. As this study is retrospective cell depletion 2 weeks after the BM cell transplantation, it would be difficult to determine the initial situation of cell contribution, that is, how much donor cell populations actually existed and distributed as CMs, ECs, or MCs. The roles and interactions of each cell population in cardiac restoration are still unclear. To provide further mechanistic insights into cardiac restoration after cell transplantation, here we performed a new attempt of prospective analysis using cell type-controlled transplantation with reassembly of defined cell populations. We succeeded in identifying that CMs play central roles in functional restoration mainly through neovascularization, and interactions among cardiovascular cells induce substantial enhancement of the angiogenic function. Our study thus can set a strategic principle for cardiac restorative therapy after MI; that is, to maximize the supply of CMs with cellular interaction to ischemic area, which can rescue missing endogenous CMs through induction of neovascularization (Supporting Information Fig. S6). In most of the current stem cell therapies, differentiation efficiency to CMs was rather low. Increasing the amount of CMs in cell therapy should be important not only for direct contribution of CMs but also for further efficient neovascularization.

In addition to neovascularization, paracrine effects after cell therapy were reported to be involved in cell survival, migration, extracellular matrix regulation, and so on. We thus further investigated other humoral factor expressions in the cell sheets (Supporting Information Fig. S7). Among the factors we tested, the following molecules showed more than a fivefold increase of mRNA expression in C + E + M sheet than that in E + M sheet: Sfrp1 (secreted frizzled-related protein 1; 8.21), Fgf2 (bFGF; 6.26), and Timp1 [tissue inhibitor of metalloproteinase-1 (TIMP1); 5.73]. Tmsb4x (Thymosin $\beta 4$) and Vcam1 [vascular cell adhesion molecule 1 (VCAM1)] expressions were also enhanced in C + E + M sheet. bFGF is well known to possess broad biological effects including angiogenesis, cardiac stem cell survival, and growth [17]. SFRP and soluble VCAM1 were reported to induce angiogenesis and suppress cell death [6, 50]. Thymosin $\beta 4$ promotes cardiac cell migration and survival [51]. Thymosin $\beta 4$ is also reported to promote induction of de novo CMs from an epicardial origin of the progenitor population in adult mouse heart after injury [52]. TIMP1 was reported to suppress apoptosis and LV remodeling after MI [53, 54]. All these factors (and others) should have a combinatorial effect on functional advantage after cardiac tissue transplantation. Detailed studies for functions and contributions of each factor would provide further understanding of the molecular mechanisms for functional improvement after cell therapy.

As a future perspective, improvements and further exploration would be expected as follows. First, a more efficient survival of transplanted cardiac tissue sheets is expected. In this study, we performed the sheet transplantation at 1 week after MI induction (subacute stage). This should be the optimal transplantation timing, avoiding damage of transplanted cell with acute inflammation and obtaining sufficient tissue repair before fibrotic scar formation in chronic stage [55, 56]. However, sufficient long-term engraftment was not achieved in this study. This may be due to xenotransplantation between mouse cells and nude rats. Although we did not observe apparent immune responses after the sheet

transplantation, a more stringent control with immunosuppressants or severer immunodeficient rat models, such as X-linked severe combined immunodeficiency (X-SCID) rats [57], may improve the survival. Otherwise, since more cells that survived were observed in peri-MI than central MI region, the severe ischemic condition at central-MI areas may not be suitable for sheet survival. Novel techniques increasing blood flow in the graft should be applied, such as prevascularization in three-dimensional tissue formation [35, 58, 59] and/or vascularized flap grafts. Furthermore, the presence of epicardium may become a physical barrier for the engraftment to host myocardium with this sheet transplantation. Arrhythmogenic potential of the engrafted CMs would be another obstacle for the clinical application. Considering these points, although the sheet transplantation is a potent option for the treatment of heart failure, further exploration for the feasibility of this new therapeutic modality would be required.

Second, the extension of the technology to iPSCs should be explored. We have already succeeded in generating cardiac tissue sheets using mouse iPSCs with the same method as that of ESCs (Supporting Information Fig. S8). We recently reported functional CM induction from human iPSCs [60]. We further established a more efficient CM induction as well as purification methods in human iPSCs [61]. EC and MC induction from human iPSCs has already been reported [62]. Technological basis to generate human cardiac tissue sheets from iPSCs has thus been established. Transplantation experiments in various animal models would prove the feasibility of human cardiac tissue sheet strategy for clinical use.

Finally, an exploration of cell-free therapy is expected. Here, we showed that cardiac tissue sheets mainly act through CM-originated paracrine effects of VEGF and other factors (Supporting Information Fig. S7) [18, 22–25]. When we could spatially and temporally reconstitute all these paracrine functions of the cardiac tissue sheets by defined humoral factors, it should be possible to reproduce the same therapeutic outcome by a cell-free factor delivery system. Such cell-free method would be more easily and broadly applicable to clinical use than cell therapy.

Conclusions

Here, we have successfully demonstrated the potentials and novel mechanisms of pluripotent stem cell-derived cardiac cell therapy with new experimental approaches. This study would provide a hallmark for cell therapy with pluripotent stem cells and strategic principle for future cardiac restoration therapy.

Acknowledgments

We thank Dr. S. Yamanaka (Center for iPS Cell Research and Application, Kyoto University) for mouse iPS cells (20D-17). We thank Dr. M. Takahashi for critical reading of the manuscript. This work was supported by research grants from the Ministry of Education, Culture, Sports, Science, and Technology, Japan, the Ministry of Health, Labor, and Welfare, Japan (to J.K.Y. and T.I.), the New Energy Industrial Development Organization of Japan, the Project for Realization of Regenerative Medicine (to J.K.Y.), the fellowship from the Japan Society for the Promotion of Science (to K.Y., H.U., and G.N.), Invited Research Project of Transnational Research Center, Kyoto University Hospital (to A.M. and R.S.), and Japan Heart Foundation Young Investigator's Research Grant (to K.Y.).

Disclosure of Potential Conflicts of Interest

T.S. is a consultant for CellSeed, Inc. T.O. is an investor in CellSeed, Inc. and an inventor/developer designated on the patent for temperature-responsive culture surfaces. The authors indicate no competing financial interests.

References

1 Orlic D, Kajstura J, Chimenti S et al. Bone marrow cells regenerate infarcted myocardium. Nature 2001;410:701–705.
2 Tomita S, Li RK, Weisel RD et al. Autologous transplantation of bone marrow cells improves damaged heart function. Circulation 1999;100:II247–II256.
3 Asahara T, Murohara T, Sullivan A et al. Isolation of putative progenitor endothelial cells for angiogenesis. Science 1997;275:964–967.
4 Murry CE, Wiseman RW, Schwartz SM et al. Skeletal myoblast transplantation for repair of myocardial necrosis. J Clin Invest 1996;98: 2512–2523.
5 Messina E, De Angelis L, Frati G et al. Isolation and expansion of adult cardiac stem cells from human and murine heart. Circ Res 2004; 95:911–921.
6 Matsuura K, Honda A, Nagai T et al. Transplantation of cardiac progenitor cells ameliorates cardiac dysfunction after myocardial infarction in mice. J Clin Invest 2009;119:2204–2217.
7 Kolossov E, Bostani T, Roell W et al. Engraftment of engineered ES cell-derived cardiomyocytes but not BM cells restores contractile function to the infarcted myocardium. J Exp Med 2006;203: 2315–2327.
8 Chien KR. Regenerative medicine and human models of human disease. Nature 2008;453:302–305.
9 Assmus B, Rolf A, Erbs S et al. Clinical outcome 2 years after intracoronary administration of bone marrow-derived progenitor cells in acute myocardial infarction. Circ Heart Fail 2010;3:89–96.
10 Hirsch A, Nijveldt R, van der Vleuten PA et al. Intracoronary infusion of mononuclear cells from bone marrow or peripheral blood compared with standard therapy in patients after acute myocardial infarction treated by primary percutaneous coronary intervention: Results of the randomized controlled HEBE trial. Eur Heart J 2011;32: 1736–1747.
11 Huikuri HV, Kervinen K, Niemelä M et al. Effects of intracoronary injection of mononuclear bone marrow cells on left ventricular function, arrhythmia risk profile, and restenosis after thrombolytic therapy of acute myocardial infarction. Eur Heart J 2008;29:2723–2732.
12 Assmus B, Fischer-Rasokat U, Honold J et al. Transcoronary transplantation of functionally competent BMCs is associated with a decrease in natriuretic peptide serum levels and improved survival of patients with chronic postinfarction heart failure: Results of the TOPCARE-CHD Registry. Circ Res 2007;100:1234–1241.
13 Tendera M, Wojakowski W, Ruzy[swsl]l[swsl]lo W et al. Intracoronary infusion of bone marrow-derived selected CD34+CXCR4+ cells and non-selected mononuclear cells in patients with acute STEMI and reduced left ventricular ejection fraction: Results of randomized, multicentre myocardial regeneration by intracoronary infusion of selected population of stem cells in acute myocardial infarction (REGENT) Trial. Eur Heart J 2009;30:1313–1321.
14 Losordo DW, Schatz RA, White CJ et al. Intramyocardial transplantation of autologous CD34+ stem cells for intractable angina: A phase I/IIa double-blind, randomized controlled trial. Circulation 2007;115: 3165–3172.
15 Menasché P, Alfieri O, Janssens S et al. The myoblast autologous grafting in ischemic cardiomyopathy (MAGIC) trial: First randomized placebo-controlled study of myoblast transplantation. Circulation 2008;117:1189–1200.
16 Dib N, Dinsmore J, Lababidi Z et al. One-year follow-up of feasibility and safety of the first U.S., randomized, controlled study using 3-dimensional guided catheter-based delivery of autologous skeletal myoblasts for ischemic cardiomyopathy (CAuSMIC study). JACC Cardiovasc Interv 2009;2:9–16.
17 Takehara N, Tsutsumi Y, Tateishi K et al. Controlled delivery of basic fibroblast growth factor promotes human cardiosphere-derived cell

engraftment to enhance cardiac repair for chronic myocardial infarction. J Am Coll Cardiol 2008;52:1858–1865.
18 Li TS, Cheng K, Malliaras K et al. Expansion of human cardiac stem cells in physiological oxygen improves cell production efficiency and potency for myocardial repair. Cardiovasc Res 2011;89:157–165.
19 Menasché P. Cardiac cell therapy: Lessons from clinical trials. J Mol Cell Cardiol 2011;50:258–265.
20 Wollert KC, Drexler H. Cell therapy for the treatment of coronary heart disease: A critical appraisal. Nat Rev Cardiol 2010;7:204–215.
21 Zimmermann WH, Melnychenko I, Wasmeier G et al. Engineered heart tissue grafts improve systolic and diastolic function in infarcted rat hearts. Nat Med 2006;12:452–458.
22 Psaltis PJ, Zannettino ACW, Worthley SG et al. Concise review: Mesenchymal stromal cells: Potential for cardiovascular repair. Stem Cells 2008;26:2201–2210.
23 Tang XL, Rokosh G, Sanganalmath SK et al. Intracoronary administration of cardiac progenitor cells alleviates left ventricular dysfunction in rats with a 30-day-old infarction. Circulation 2010;121:293–305.
24 Cho HJ, Lee N, Lee JY et al. Role of host tissues for sustained humoral effects after endothelial progenitor cell transplantation into the ischemic heart. J Exp Med 2007;204:3257–3269.
25 Kocher AA, Schuster MD, Szabolcs MJ et al. Neovascularization of ischemic myocardium by human bone-marrow derived angioblasts prevents cardiomyocyte apoptosis, reduces remodeling and improves cardiac function. Nat Med 2001;7:430–436.
26 Mirotsou M, Jayawardena TM, Schmeckpeper J et al. Paracrine mechanisms of stem cell reparative and regenerative actions in the heart. J Mol Cell Cardiol 2011;50:280–289.
27 Joggerst SJ, Hatzopoulos AK. Stem cell therapy for cardiac repair: Benefits and barriers. Expert Rev Mol Med 2009;11:e20.
28 Yamashita J, Itoh H, Hirashima M et al. Flk1-positive cells derived from embryonic stem cells serve as vascular progenitors. Nature 2000; 408:92–96.
29 Yamamizu K, Kawasaki K, Katayama S et al. Enhancement of vascular progenitor potential by protein kinase A through dual induction of Flk-1 and Neuropilin-1. Blood 2009;114:3707–3716.
30 Yamashita JK, Takano M, Hiraoka-Kanie M et al. Prospective identification of cardiac progenitors by a novel single cell-based cardiomyocyte induction. FASEB J 2005;19:1534–1536.
31 Narazaki G, Uosaki H, Teranishi M et al. Directed and systematic differentiation of cardiovascular cells from mouse induced pluripotent stem cells. Circulation 2008;118:498–506.
32 Pelacho B, Mazo M, Gavira JJ et al. Adult stem cells: From new cell sources to changes in methodology. J Cardiovasc Transl Res 2011;4: 154–160.
33 Okano T, Yamada N, Sakai H et al. A novel recovery system for cultured cells using plasma-treated polystyrene dishes grafted with poly (*N*-isopropylacrylamide). J Biomed Mater Res 1993;27:1243–1251.
34 Bel A, Planat-Bernard V, Saito A et al. Composite cell sheets: A further step toward safe and effective myocardial regeneration by cardiac progenitors derived from embryonic stem cells. Circulation 2010;122: S118–S123.
35 Sekine H, Shimizu T, Hobo K et al. Endothelial cell coculture within tissue-engineered cardiomyocyte sheets enhances neovascularization and improves cardiac function of ischemic hearts. Circulation 2008; 118:S145–S152.
36 Miyahara Y, Nagaya N, Kataoka M et al. Monolayered mesenchymal stem cells repair scarred myocardium after myocardial infarction. Nat Med 2006;12:459–465.
37 Yan P, Nagasawa A, Uosaki H et al. Cyclosporin-A potently induces highly cardiogenic progenitors from embryonic stem cells. Biochem Biophys Res Commun 2009;379:115–120.
38 Yurugi-Kobayashi T, Itoh H, Schroeder T et al. Adrenomedullin/cyclic AMP pathway induces Notch activation and differentiation of arterial endothelial cells from vascular progenitors. Arterioscler Thromb Vasc Biol 2006;26:1977–1984.
39 Nishina T, Nishimura K, Yuasa S et al. Initial effects of the left ventricular repair by plication may not last long in a rat ischemic cardiomyopathy model. Circulation 2001;104:I241–I245.
40 Sakakibara Y, Tambara K, Lu F et al. Combined procedure of surgical repair and cell transplantation for left ventricular aneurysm: An experimental study. Circulation 2002;106:I193–I197.
41 Pacher P, Nagayama T, Mukhopadhyay P et al. Measurement of cardiac function using pressure-volume conductance catheter technique in mice and rats. Nat Protoc 2008;3:1422–1434.
42 Nishiyama N, Miyoshi S, Hida N et al. The significant cardiomyogenic potential of human umbilical cord blood-derived mesenchymal stem cells in vitro. Stem Cells 2007;25:2017–2024.
43 Young DM, Greulich KM, Weier HG. Species-specific in situ hybridization with fluorochrome-labeled DNA probes to study vascularization of human skin grafts on athymic mice. J Burn Care Rehabil 1996;17:305–310.
44 Ieda M, Tsuchihashi T, Ivey KN et al. Cardiac fibroblasts regulate myocardial proliferation through β1 integrin signaling. Dev Cell 2009; 16:233–244.
45 Miragoli M, Gaudesius G, Rohr S. Electrotonic modulation of cardiac impulse conduction by myofibroblasts. Circ Res 2006;98:801–810.
46 Olivetti G, Capasso JM, Meggs LG et al. Cellular basis of chronic ventricular remodeling after myocardial infarction in rats. Circ Res 1991;68:856–869.
47 Pfeffer MA, Braunwald E. Ventricular remodeling after myocardial infarction. Experimental observations and clinical implications. Circulation 1990;81:1161–1172.
48 Braunwald E. Myocardial reperfusion, limitation of infarct size, reduction of left ventricular dysfunction, and improved survival. Should the paradigm be expanded? Circulation 1989;79:441–444.
49 Yoon CH, Koyanagi M, Iekushi K et al. Mechanism of improved cardiac function after bone marrow mononuclear cell therapy: Role of cardiovascular lineage commitment. Circulation 2010;121:2001–2011.
50 Dufourcq P, Leroux L, Ezan J et al. Regulation of endothelial cell cytoskeletal reorganization by a secreted frizzled-related protein-1 and Frizzled 4- and Frizzled 7-dependent pathway: Role in neovessel formation. Am J Pathol 2008;172:37–49.
51 Bock-Marquette I, Saxena A, White MD et al. Thymosin beta4 activates integrin-linked kinase and promotes cardiac cell migration, survival and cardiac repair. Nature 2004;432:466–472.
52 Smart N, Bollini S, Dubé KN et al. De novo cardiomyocytes from within the activated adult heart after injury. Nature 2011;474: 640–644.
53 Hornebeck W. Down-regulation of tissue inhibitor of matrix metalloprotease-1 (TIMP-1) in aged human skin contributes to matrix degradation and impaired cell growth and survival. Pathol Biol 2003;51: 569–573.
54 Ikonomidis JS, Hendrick JW, Parkhurst AM et al. Accelerated LV remodeling after myocardial infarction in TIMP-1-deficient mice: Effects of exogenous MMP inhibition. Am J Physiol Heart Circ Physiol 2005;288:H149–H158.
55 Li RK, Mickle DAG, Weisel RD et al. Optimal time for cardiomyocyte transplantation to maximize myocardial function after left ventricular injury. Ann Thorac Surg 2001;72:1957–1963.
56 Sumitra M, Manikandan P, Nayeem M et al. Time course studies on the initiation of complement activation in acute myocardial infarction induced by coronary artery ligations in rats. Mol Cell Biochem 2005; 268:149–158.
57 Mashimo T, Takizawa A, Voigt B et at. Generation of knockout rats with X-linked severe combined immunodeficiency (X-SCID) using zinc-finger nucleases. PLoS One 2010;5:e8870.
58 Sekiya S, Muraoka M, Sasagawa T et al. Three-dimensional cell-dense constructs containing endothelial cell-networks are an effective tool for in vivo and in vitro vascular biology research. Microvasc Res 2010;80:549–551.
59 Stevens KR, Kreutziger KL, Dupras SK et al. Physiological function and transplantation of scaffold-free and vascularized human cardiac muscle tissue. Proc Natl Acad Sci USA 2009;106:16568–16573.
60 Fujiwara M, Yan P, Otsuji TG et al. Induction and enhancement of cardiac cell differentiation from mouse and human induced pluripotent stem cells with cyclosporin-A. PLoS One 2011;6:e16734.
61 Uosaki H, Fukushima H, Takeuchi A et al. Efficient and scalable purification of cardiomyocytes from human embryonic and induced pluripotent stem cells by VCAM1 surface expression. PLoS One 2011;6: e23657.
62 Taura D, Sone M, Homma K et al. Induction and isolation of vascular cells from human induced pluripotent stem cells—Brief report. Arterioscler Thromb Vasc Biol 2009;29:1100–1103.


See www.StemCells.com for supporting information available online.

Bone 50 (2012) 69–78

Contents lists available at SciVerse ScienceDirect

Bone

journal homepage: www.elsevier.com/locate/bone

Original Full Length Article

Id2 controls chondrogenesis acting downstream of BMP signaling during maxillary morphogenesis

Tomoko Sakata-Goto [a], Katsu Takahashi [a,*], Honoka Kiso [a], Boyen Huang [a], Hiroko Tsukamoto [a], Mitsuru Takemoto [b], Tatsunari Hayashi [c], Manabu Sugai [c], Takashi Nakamura [b], Yoshifumi Yokota [d], Akira Shimizu [c], Harold Slavkin [e], Kazuhisa Bessho [a]

[a] Department of Oral and Maxillofacial Surgery, Graduate School of Medicine, Kyoto University, Japan
[b] Department of Orthopedic Surgery, Kyoto University Hospital, Japan
[c] Translation Research Center, Kyoto University Hospital, Japan
[d] Division of Molecular Genetics, Department of Biochemistry and Bioinformative Sciences, Faculty of medical Sciences, University of Fukui, Japan
[e] Center for Craniofacial Molecular Biology, School of Dentistry, University of Southern California, USA

ARTICLE INFO

Article history:
Received 3 June 2011
Revised 3 September 2011
Accepted 16 September 2011
Available online 1 October 2011

Edited by: R. Baron

Keywords:
Id2
Synchondrosis
BMP
Smad7
Jaw deformity

ABSTRACT

Maxillofacial dysmorphogenesis is found in 5% of the population. To begin to understand the mechanisms required for maxillofacial morphogenesis, we employed the inhibitors of the differentiation 2 (Id2) knock-out mouse model, in which Id proteins, members of the regulator of basic helix–loop–helix (bHLH) transcription factors, modulate cell proliferation, apoptosis, and differentiation.

We now report that spatially-restricted growth defects are localized at the skull base of Id2 KO mice. Curiously, at birth, neither the mutant Id2 KO nor wild-type (WT) mice differed, based upon cephalometric and histological analyses of cranial base synchondroses. In postnatal week 2, a narrower hypertrophic zone and an inhibited proliferative zone in presphenoid synchondrosis (PSS) and spheno-occipital synchondrosis (SOS) with maxillary hypoplasia were identified in the Id2 mutant mice. Complementary studies revealed that exogenous bone morphogenetic proteins (BMPs) enhanced cartilage growth, matrix deposition, and chondrocyte proliferation in the WT but not in the mutant model. Id2-deficient chondrocytes expressed more Smad7 transcripts.

Based on our results, we assert that Id2 plays an essential role, acting downstream of BMP signaling, to regulate cartilage formation at the postnatal stage by enhancing BMP signals through inhibiting Smad7 expression. As a consequence, abnormal endochondral ossification was observed in cranial base synchondroses during the postnatal growth period, resulting in the clinical phenotype of maxillofacial dysmorphogenesis.

Introduction

Temporal and spatial information is critical for craniofacial morphogenesis, especially between forming the mandible and complementary maxilla. In human craniofacial development, morphospatial disharmony between the maxillocranial and mandibular complex results in well-recognized jaw deformities, including maxillary hypoplasia, mandibular prognathism, mandibular micrognathism, and facial asymmetry [1]. Patients with severe jaw deformities present significant masticatory dysfunctions and severe psychosocial issues. Such patients require surgical correction and postsurgical rehabilitation. The prevalence of such jaw deformities ranges from 1 to 23% according to the ethnic background of study populations [2–5]. Jaw deformities become apparent after birth, as well as being associated with first and second branchial arch syndromes, including Treacher Collins syndrome, Pierre Robin syndrome, Crouzon syndrome, cleidocranial dysplasia (CCD), achondroplasia, and Pfeiffer syndrome. These relatively rare branchial arch syndromes are readily identified at birth, and these represent less than 5% of jaw deformity cases [1]. The vast majority of such cases become clinically evident during early postnatal growth and development. Overt manifestation of the postnatal jaw deformities may not appear until after adolescence, being generally associated with increased craniofacial growth. Both environmental and genetic factors have been identified as causes of postnatal jaw deformities [6,7], and available evidence suggests that genetic factors are the major determinants to the clinical phenotype [8–10]. However, the primary cause for maxillofacial dysmorphogenesis is not known.

In order to investigate growth impairment in postnatal jaw deformities, we identified the role of cartilages in the growth and development of the craniofacial complex. Available evidence suggests that SOS and nasal septal cartilage (NSC) are derived from the chondrocranium

* Corresponding author at: Katsu Takahashi: Shogoin-Kawahara-cho 54, Sakyo-ku, Kyoto, 606-8507, Japan. Fax: +81 75 761 9732.
E-mail address: takahask@kuhp.kyoto-u.ac.jp (K. Takahashi).

8756-3282/$ – see front matter © 2011 Elsevier Inc. All rights reserved.
doi:10.1016/j.bone.2011.09.049

[11]. Multiple synchondroses separating bones of the skull base are assumed to function as growth sites during skull base expansion. Morphologically, a synchondrosis appears at two opposing cartilage growth plates. Therefore, analogous to endochondral growth plates in long bones, synchondroses of the skull base develop through aberrations of the temporal and spatial combination of chondrocyte proliferation and hypertrophy [7]. In a mouse model, both the PSS and SOS remain patent through adulthood. Similar to the epiphyseal growth plate in long bones, the cell proliferation, differentiation, and maturation rates of chondrocytes within synchondroses are critical for the longitudinal growth of the cranial base [12].

Id proteins are members of the regulator of helix–loop–helix (HLH) transcription factors [13–15]. Transcriptional regulators with a bHLH domain regulate a broad range of cellular differentiation processes including myogenesis, neurogenesis, and hematopoiesis [16]. In embryonic and adult tissues, Id proteins act as regulators of cell proliferation, differentiation, tumorigenesis, and neoplastic transformation [17–19]. Id expression is partially regulated by BMP-Smad signaling [20,21]. BMP regulates cell fate determination, differentiation, proliferation, maturation, hypertrophy, and apoptosis of chondrocyte cells [22]. The mechanisms by which BMPs control specific cell lineages and patterns have been found to be critical for subsequent stages of development [23]. The exogenous application of BMP2 or BMP4 to embryonic maxillary mesenchymal cells resulted in a significant upregulation of Id1, Id2, and Id3 mRNA [24] and the modulation of Id1, Id2, Id3, as well as Id4 protein levels [25]. BMP2 and BMP4 induced the transcription of Id1, Id2, and Id3 genes in ES cells as well as embryos by promoting the direct binding of the BMP-responsive Smads; Smad1 and Smad5 binding to promoters of these genes [26–28]. This body of evidence suggests important functions of Id proteins during postnatal jaw growth and development.

First, we identified maxillary hypoplasia in Id2 KO mice. We advanced the hypothesis that Id2 abrogation will interfere with the transduction of BMP signaling and, thereby, contributes to maxillary hypoplasia due to abnormal endochondrial ossification in the cranial base synchondrosis during the postnatal growth period. To test our hypothesis, we utilized the Id2 KO mouse model.

Materials and methods

Mice

Id2 mutant mice [14], with a 129/Sv genetic background, were bred under a specific pathogen-free condition and used in this study. All experimental procedures were carried out according to the guidelines for animal experiments regulated by Kyoto University Graduate School of Medicine.

Image analysis of skulls

Neonatal and postnatal mice at the ages of 0, 2, and 12 weeks, respectively, were sacrificed with carbon dioxide gas. The skulls were then analyzed employing an X-ray microtomography method (SMX-100CT-SV3, Shimadzu Co., Kyoto, Japan). The means of the three-dimensional coordinates of these landmarks were used for image analyses of the skull. EDMA was used to measure localized differences between Id2 KO mice and the control group, as described previously [29]. A nonparametric statistical technique was used to evaluate the significance of differences [29].

Analysis of cell proliferation and apoptosis

BrdU (5-Bromo-2′-deoxyuridine, 05650) was injected intraperitoneally at a concentration of 50 μg/g body weight 2 h before sacrifice. Target skeletal tissues were harvested, fixed overnight at 4 °C in a 4% paraformaldehyde solution, and then decalcified in a 0.5 M EDTA solution for 2 weeks. Decalcified samples were embedded in paraffin and sectioned. BrdU-positive cells were detected with BrdU antibody. The rate calculated by expressing the number of BrdU-positive nuclei as a percentage of the total number of nuclei was defined as the proliferation index. Data are presented as the mean ± SD, and further examined with Student's *t*-test. Significance was set at 5%. Apoptotic cells were visualized and identified with the ApopTaq Plus Fluorescein In Situ Apoptosis Detection Kit S7111 (CHEMICON, USA and Canada).

In situ hybridization

In situ hybridization was performed as described previously [30]. Mouse cDNA clones were: Id2 (nt.650-939; NM010496); collagenX (nt.2893-3550; NM009925); and osteopontin (nt.486-844;NM009263).

Immunohistochemistry

Paraffin-embedded sections were subjected to immunostaining with goat polyclonal antibodies directed against Col2 (1:100) (code: 1320-01/SBA), rabbit serum against Col10 (1:200) (code: LB-0092/Lot: 812021/LSL), and primary rabbit antibodies against phosphorylated Smad 1/5/8 (1:100) (Cell Signaling Technology, MA, USA) [31].

Semi-quantitative RT-PCR analysis

Total RNA was cultured with TRIzol (Gibco-BRL, Gaitherburg, MD, USA), according to the manufacturer's instructions, and then quantitated with A260. Oligo(dT)-primed cDNA was prepared with a reverse transcriptase. For the purpose of semiquantitation, 50 ng of cDNA was serially diluted and subjected to PCR amplification with primer pairs. These primer pairs were: Id2, sense, 5′-AGCATCCCCCAGAACAAGAAGGTG-3′ and antisense, 5′-ATCGTCTTGCCCAGGTGTCGTTCT-3′; GAPDH, sense, 5′-CCATCACATCTTCCAGGAG-3′ and antisense, 5′-CCTGCTTCACCACCTTCTTG-3′; BMPR1, sense, 5′-CCTGTTGTTATAGGTCCGTTCTTTG-3′ and antisense, 5′-CGCCATTTACCCATCCATACTT-3′; BMPR2, sense, 5′-CTAACTGGAAATCGGCTGGTG-3′ and antisense, 5′-TGGGTCTCTGCTTCTCTCTGG-3′; Smad1, sense, 5′-AGCCTCTGGAATGCTGTGAGTT-3′ and antisense, 5′-TGGTTGGGGAGTGAGGGTAG-3′; Smad5, sense, 5′-TATGCCAGAACCACAGAAAGGA-3′ and antisense, 5′-ACAGCAAGAGAGGCAGGACTATG-3′; Smad6, sense, 5′-TGCTCAGCAAGGAGCCAGAC-3′ and antisense, 5′-CTGTGGTTGTTGAGTAGGATCTCCA-3′; Smad7, sense, 5′-TGCAGGCTGTCCAGATGCT-3′ and antisense, 5′-CTTGATGGAGAAACCAGGGAAC-3′. All PCR products were examined employing an electrophoretical technique that used 2% agarose gel and ethidium bromide staining. These bands were quantitated with a Bio-image analyzer (Fujix BAS2000, Fuji Photo Film, Tokyo, Japan). All the PCR data were representative from three independent experiments.

Microdissection and organ culture

P7 wild-type mice cranial base structures were dissected in Dulbecco's PBS (pH = 7.4) under a stereomicroscope. The dissected structures were cultured on Nucleopore filters at 37 °C, under a 5% carbon dioxide atmosphere, in a trowel-type organ culture containing BGJb supplemented with 200 ng/ml of BMP-2, BMP-4, and BMP-7 (R&D Systems, MN, USA). The culture medium was renewed every 2 days [31]. After the culture, explants were fixed in a 4% para-formaldehyde and formalin solution, and then processed for histological and immunohistochemical examinations.

Results

Id2 abrogation results in retarded postnatal growth of the maxillofacial complex

Adult Id2-deficient mice showed a shorter maxillofacial profile (Figs. 1A–I). Id2 KO mice present severe clinical phenotypes with

anterior transverse crossbite (Figs. 1A, B and E). The Id2 heterozygous mice showed phenotypically normal profile. We attempted to quantitate the malformation by Euclidean Distance Matrix Analysis (EDMA) to measure and compare the three-dimensional differences between 12-week-old Id2 KO mice, and the control group. We used in these morphometric studies the 89 distances between specific points (Supplemental Figs. 1 and 2). Nasal and frontal bones of Id2 mutants were disproportionally shortened in 32 distances (Fig. 1H). Significant

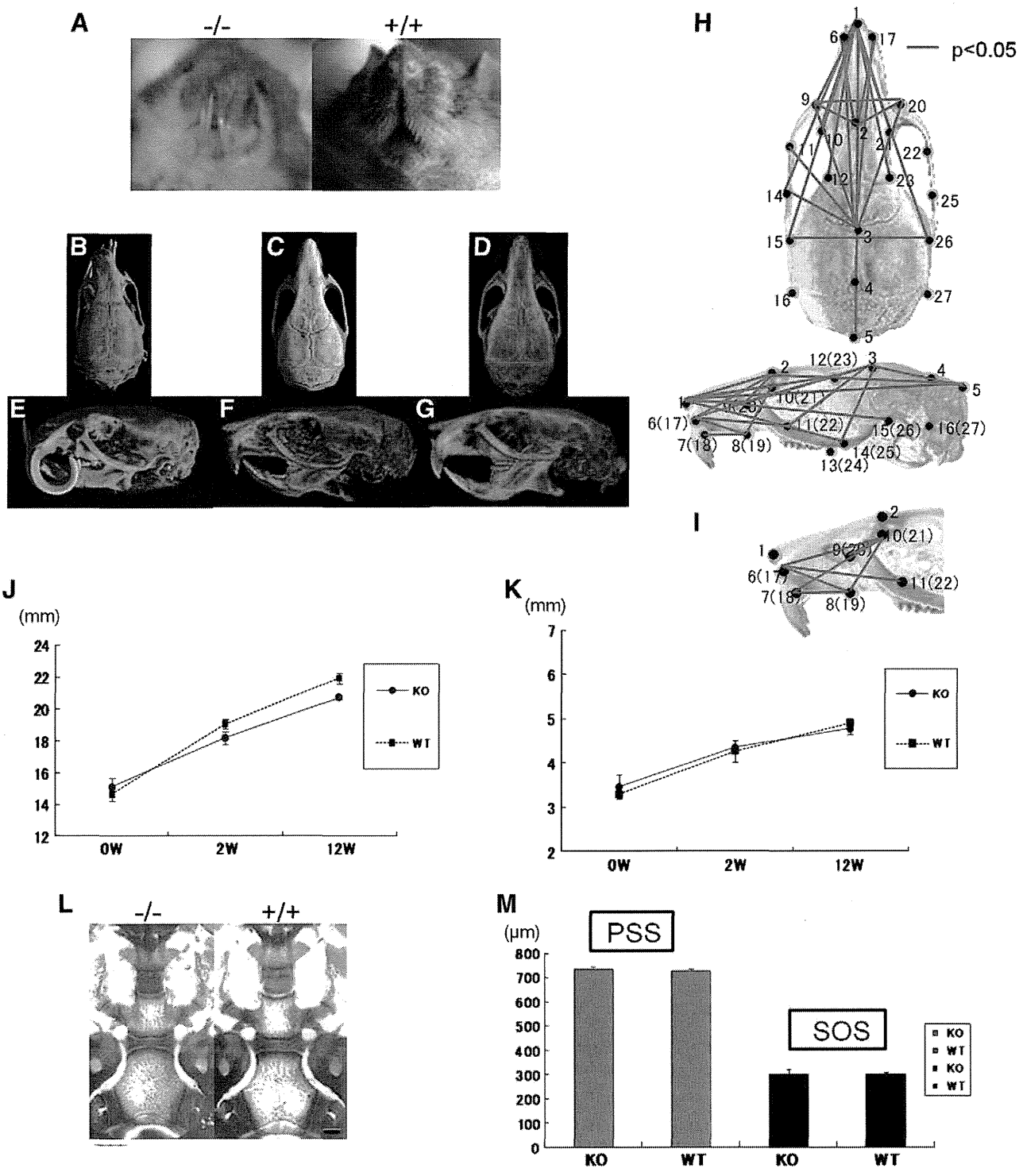

Fig. 1. The shorter maxillofacial profile in adult Id2-deficient mice. Comparison of the Id2 KO and control groups in week 12. (A) Facial differences between Id2 KO (right panel) and the control (left panel). Superior view of adult mouse skulls: Id2 KO (severe case) (B), Id2 KO (mild case) (C), and the control (D). Lateral view of adult mouse skulls: Id2 KO (severe case) (E), Id2 KO (mild case) (F), and the control (G). (H) Measurement of the cranial dimensions. Landmarks used for cranial measurements were based on those used by Arron JR et al. (Supplemental Fig. 1) [29]. The red lines indicate significantly different distances between Id2 KO and the wild-type. $p<0.05$ using Student's *t*-test. (I) Detailed measurement of the premaxilla and maxilla. The red lines indicate significantly different distances between Id2 KO and the wild-type. $p<0.05$ using Student's *t*-test. The longitudinal distance between the nasal and intersection of the interparietal and occipital bones at the midline (J), and the width of the bilateral frontal-squamosal intersection at the temporal crest, with age (K). (L) Alizarin red and Alcian blue staining did not differentiate the Id2 KO from the control skull base. (M) The length of the presphenoid synchondrosis (gray bar) and spheno-occipital synchondrosis (black bar) did not differ between the two groups ($n=3$). All error bars indicated one standard deviation of uncertainty.

differences were noted in the distances between the (a) nasal and intersection of interparietal and occipital bones at the midline (1–5), (b) nasal and frontal-squamosal intersection at the temporal crest (1-12(23)), (c) nasal and intersection of the frontal process of the maxilla with frontal and lacrimal bones(1-10(21)), (d) bregma and anterior-most point at the intersection of premaxillae and nasal bones(3-6(17)), and (e) bregma and anterior notch on the frontal process lateral to the infraorbital fissure(3-9(20)). In summary, landmarks in the premaxilla and maxilla of Id2 mutant mice were influenced in what appeared to be a longitudinal direction (Fig. 1I). Importantly, there were no differences in the skull width between KO and WT mice after birth were observed (Figs. 1H and K). The difference in the longitudinal diameter between the two groups increased with age (Fig. 1J). To explore the relationship between embryonic development and maxillary hypoplasia in Id2-deficient mice, newborn pups were examined. Newborn Id2-deficient mice were not different from their WT counterparts in appearance, Alizarin red and Alcian blue staining, and EDMA (Fig. 1L). These results indicated that the severity of maxillary hypoplasia or dysmorphogenesis in Id2-deficient mice increased with postnatal growth and development. Curiously, the cranio-maxillofacial region of newborn mice was found to be essentially identical between WT and mutant.

Abnormal differentiation of the synchondrosal growth plate is caused by Id2 abrogation

PSS and SOS are important growth centers of the cranio-maxillofacial skeleton, and appear to influence the temporal and positional cues for the growth and development of the maxilla [7,32,33]. There were no differences in PSS and SOS between newborn as well as adult KO and WT mice (Fig. 1M). However, the zone of hypertrophic chondrocytes in the cranial base was narrower in the 2-week-old Id2 KO than the WT group (Figs. 2C and D). To assess the hypertrophy of chondrocytes, type X collagen (a molecular marker of the hypertrophic zone) and osteopontin (a molecular marker of the calcified zone) expressions were examined. Similar to the histological results, the distribution of type X collagen was down-regulated in Id2-deficient mice, whereas osteopontin was similarly distributed in the KO and WT tissue samples (Figs. 2G–J). The total length of SOS in Id2-deficient mice was reduced when compared to WT (Fig. 2K). These results suggest that abnormal postnatal growth of the cranial base in mutant Id2 mice resulted from the disturbed hypertrophy of chondrocytes in synchondroses.

Reduced proliferative activity of synchondrosal chondrocytes in Id2 KO mice

The proliferative activity of chondrocytes in synchondroses of the cranial base was examined employing a BrdU labeling method. The number of dividing cells in the proliferative zone of 2-week-old mutant PSS and SOS significantly decreased (Figs. 3A: a–d and B). Proliferation was reduced in the nasal septal cartilage of KO mice (Fig. 3A: e–h). Apoptosis within synchondroses was examined with a TUNEL method. Both mutant and control groups failed to display the apoptosis of chondrocytes (Fig. 3C).

Expression of Id2 in the synchondrosis of the cranial base

The expression of Id2 mRNA in the synchondrosis of the cranial base was evaluated using a semi-quantitative RT-PCR method. Id2

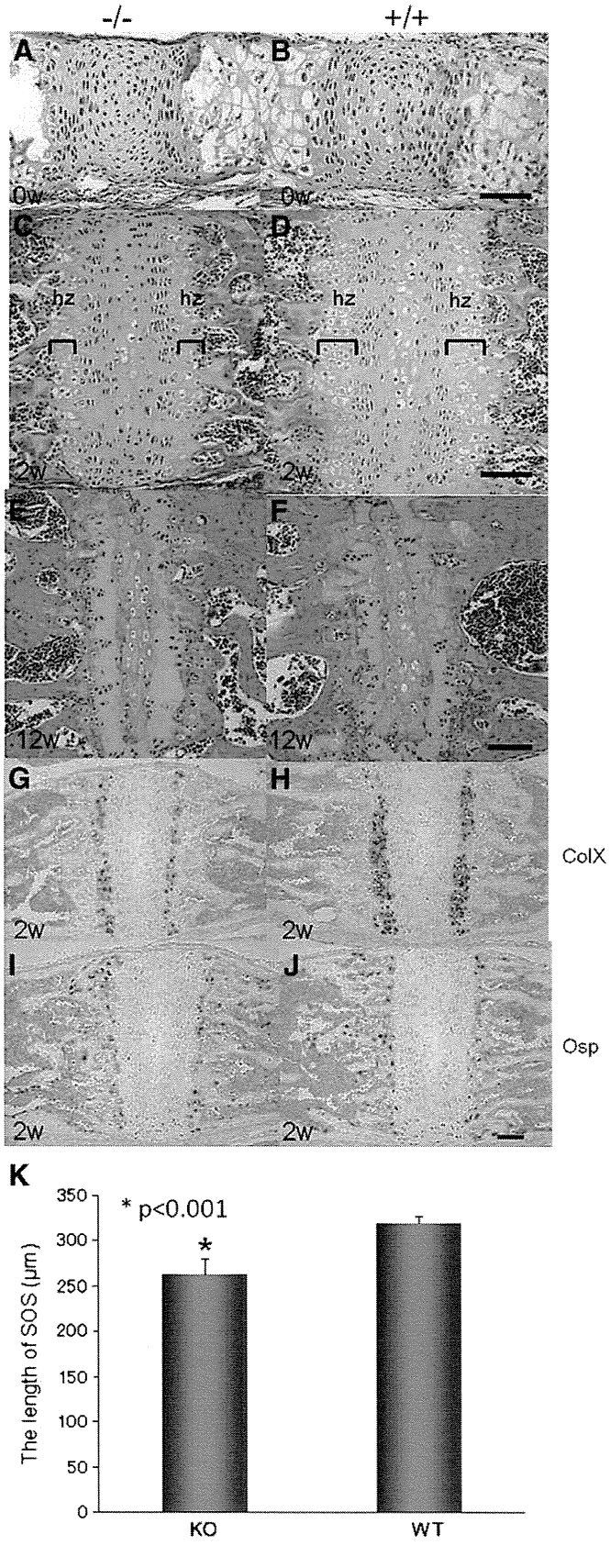

Fig. 2. Abnormal differentiation of the synchondrosal growth plate caused by the absence of Id2. In week 0, the Id2 KO and control groups did not show a difference in SOS (A and B). In week 2, the two groups revealed a difference in hypertrophic chondrocytes of SOS (C and D). In week 12, the two groups showed no difference in SOS (E and F). In week 2, the expression pattern of type X collagen in the two groups showed a difference of hypertrophic chondrocytes in SOS (G and H) visualized by in situ hybridization. In week 2, expression patterns of osteopontin in the two groups did not differ in SOS (I and J) visualized by in situ hybridization. (hypertrophic zone (hz): bracket. Scale bar: 100 μm). (K) The length of the SOS in transverse sections of Id2-deficient (left bar) as well as wild-type (right bar) mice is shown as an average length. Five sections were prepared from five different mice. All error bars are standard deviations of uncertainty. $p<0.001$ by Student's *t*-test.

transcript expression in the cranial base was significant in postnatal facial development, and kept the same level in 2-week, 4-week, 6-week or 12-week-old after birth (Fig. 4A: a). Id2 is also expressed in many adult tissues including spleen, brain, liver, bone marrow, heart and kidney (Fig. 4A: b). Analyses of in situ hybridization showed that Id2 was ubiquitously expressed in all portions of synchondroses, including the proliferating and hypertrophic zones (Fig. 4B). This was interpreted to mean that Id2 expression in synchondroses was detected but not localized to a specific region.

Suppressed chondrocyte proliferation and differentiation on exposure to exogenous BMPs in the cranial base of Id2 KO mice in vitro

Id expression is regulated by a BMP-Smad signaling pathway. We assayed the functions of BMP2, BMP4, and BMP7 in the cranial base in vitro. The cranial bases were isolated from 7-day-old mice, which referred to the postnatal growing and developmental stage, and divided into three groups: treated with exogenous BMP2 (200 ng/ml), BMP4 (200 ng/ml), or BMP7 (200 ng/ml) every 2 days for three continuous cycles (total: 6 days) (Fig. 5A: a–h). In the BMP2 and BMP4 groups, an additional increase in the PSS length of Id2 WT cranial bases was observed (Figs. 5A: d and f and B). Histochemical analyses of type II and X collagen were conducted. In the presence of exogenous BMP2, the degree of chondrocyte hypertrophy from Id2 WT cranial bases increased (Figs. 5D and F: d–f). The application of BMP2 failed to cause a difference in the degree of chondrocyte hypertrophy between Id2 KO and control cranial bases (Figs. 5C and E: d–f). The degrees of chondrocyte hypertrophy adjacent to the bone and ectopic hypertrophy surrounding the central reserve zone of synchondroses increased in the Id2 WT group receiving exogenous BMP4 (200 ng/ml) (Figs. 5D and F: g–i). The increase of the hypertrophy due to the application of BMP4 did not differ between Id2 KO and control cranial bases (Figs. 5C and E: g–i). In the BMP7 group, the amount of proliferative chondrocytes from Id2 WT cranial bases increased (Figs. 5D and F: j–l). No other differences between Id2 KO and control cranial bases were identified in the BMP7 group

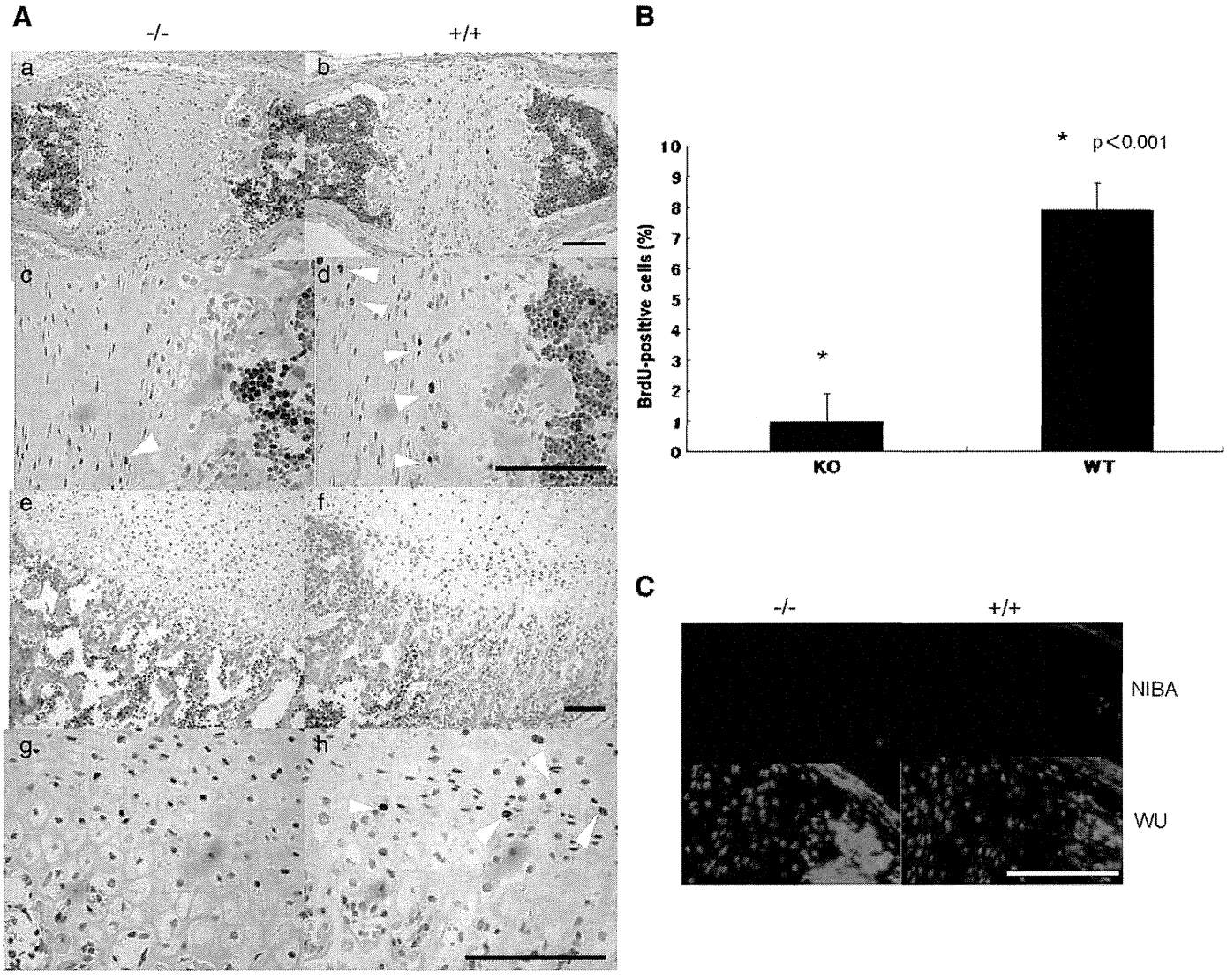

Fig. 3. Reduced proliferative activity of synchondrosal chondrocytes in Id2-deficient mice. (A) The reduction of chondrocyte proliferation in Id2 KO PSS and NSC. Sagittal view of 2-week-old PSS in the Id2 KO and control cranial base (a–d); lower (a, b) and higher (c, d) magnification. The white arrow-head indicates BrdU-positive cells (c, d). Sagittal view of 2-week-old NSC in the Id2 KO and control (e–h); lower (e, f) and higher (g, h) magnification. The white arrowhead indicates BrdU-positive cells (h). The number of BrdU-positive cells. (B) The proliferative rate of the Id2 KO (left bar) and control (right bar) PSS chondrocytes is shown as an average percent of BrdU-positive cells relative to the total cell count. Three sections were prepared from three different mice. All error bars are standard deviations of uncertainty. $p<0.05$ by Student's *t*-test. (C) No apoptotic cells in Id2 KO presphenoid and spheno-occipital synchondrosis. Sagittal view of 2-week-old presphenoid synchondrosis in the Id2 KO and control cranial base (a–d); NIBA (a, b) and WU (c, d) images. All scale bars: 100 μm.

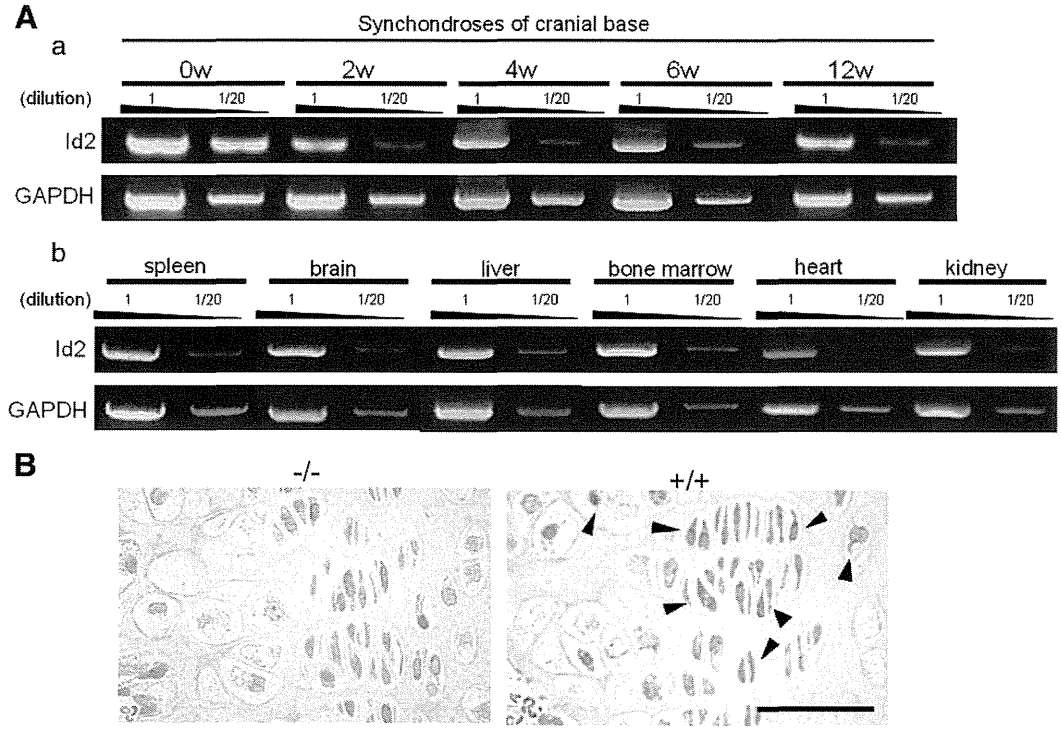

Fig. 4. Expression of Id2 in the cranial base synchondrosis. (A) Semi-quantitative RT-RCR analysis of Id2 expression in the cranial base synchondrosis. RNA was purified from the cranial base synchondrosis of 0-, 2-, 4-, 6-, and 12-week-old WT mice (a), and spleen, brain, liver, bone marrow, heart and kidney of 12-week-old WT mice (b). RT products were twentyfold serially diluted and subjected to PCR. Reduced glyceraldehyde-phosphate dehydrogenase (GAPDH) was used as an internal control. (B) In week 2, Id2 was detected in the cranial base synchondrosis, especially in proliferative and hypertrophic chondrocytes, using section in situ hybridization (black arrowhead). Scale bar: 50 μm.

(Figs. 5C and E: j–l). Exogenous BMPs enhanced chondrocyte differentiation and proliferation in the WT but not in the mutant model.

Id2 regulates BMP signaling in synchondrosis of the cranial base through inhibiting Smad7 expression

In order to identify the downstream target gene of Id2 in synchondrosis of the cranial base, we evaluated levels of expression of BMP signaling molecules including BMPR-I, BMPR-II, and several different kind of Smads. The expression of mRNAs in the synchondrosis of the cranial base within Id2 WT and KO mice was evaluated using a semi-quantitative RT-PCR method. We discovered more than five-fold up-regulation of the Smad7 transcripts, which belonged to inhibitory Smad, within the Id2-deficient mice samples (Fig. 6A). Furthermore, in order to assess whether the up-regulation of Smad7 in Id2-deficient mice is attributable to the inhibition of BMP signaling, the phosphorylation of Smad 1,5,8 was examined. Compared with the wild type, Id2-deficient mice exhibited the decreased phosphorylation of Smad 1,5,8-positive cells in chondrocytes within the synchondrosis of the cranial base (Figs. 6B and C). These data indicate Id2 controls chondrogenesis during early postnatal maxillary and mandibular growth and development by acting downstream of BMP signaling to regulate chondrocyte proliferation and differentiation and by enhancing BMP signaling through inhibiting Smad7 expression (Fig. 7).

Discussion

The results from our study clearly suggest that maxillary hypoplasia in Id2-deficient mice is a postnatal growth and development disorder. The Id2 KO mouse model presents a clinical phenotype similar to the more prevalent postnatal type of jaw deformity observed in humans. Mandibular prognathism (MP), appearing with a larger mandible, a smaller maxilla (maxillary hypoplasia), or a combination of both manifestations, has been considered a representative phenotype of jaw deformities in humans. In rare situations, MP is one of the manifestations of a syndrome, whereas most MP cases do not appear to be accompanied with other disorders.

The Mendelian inheritance patterns for postnatal jaw deformities, such as MP, are not well understood. Examples in the literature contain a variety of inheritance patterns for MP — an autosomal-recessive inheritance, autosomal-dominant inheritance, dominant inheritance with incomplete penetrance, and a polygenic model of transmission [9,34]. The actual mechanism is not as yet known. Recently, genome-wide linkage studies identified a number of MP susceptibility loci including 1p36, 6q25, 19p13.2 [10], 1p22.1, 3q26.2, 11q22, 12q13.13, 12q23 [35], and 4p16.1 [10] in MP pedigrees of Japanese as well as Korean, Hispanic Colombian, and Han Chinese, respectively.

Meanwhile, a mouse model for genetically manipulating MP has not previously been reported. Our study is the first to illustrate a

Fig. 5. BMP-2, -4, and -7 promoted chondrocyte hypertrophy and proliferation in synchondroses of the cranial base in WT but not in Id2 KO mice in vitro. (A) On postnatal day 7, cranial base explants cultured under serum-free conditions to induce in vitro development were exposed to 200 ng/ml of BMP2 (c and d), BMP4 (e and f), and BMP7 (g and h). BMP2 and BMP4 enhanced chondrocyte hypertrophy in the control (white arrowheads). (B) The length of the PSS of Id2-deficient (gray bar) as well as wild-type (black bar) mice on day 6 of organ culture is shown as an average length. Each average length of the PSS was calculated from three different explants. All error bars are standard deviations of uncertainty. $p<0.05$ by Student's *t*-test. Low magnification of Id2-deficient (C) and wild-type mice (D). High magnification of Id2-deficient (E) and wild-type mice (F). Mid-sagittal sections of PSS were stained with H&E (C–F: a, d, g, and j), immunostained for type II collagen (C–F: b, e, h, and k), or type X collagen (C–F: c, f, i, and l). The section was respectively, control (C–F: a–c) and exposed to BMP2 (C–F: d–f), BMP4 (C–F: g–i), and BMP7 (C–F: j–l). BMP2 and BMP4 enhanced chondrocyte hypertrophy (E: d–i and F: d–i). BMP7 enhanced chondrocyte proliferation (F: j–l) (hypertrophic zone (hz): bracket; proliferative zone (pz): bracket; ectopic hypertrophy: asterisks). All scale bars: 100 μm.

mouse model for postnatal jaw deformities. This model provides an opportunity to explore the molecular mechanisms underlying jaw deformity, with particular emphasis on maxillary hypoplasia.

The synchondrosis of the cranial base is an important growth center of the craniofacial skeleton, and provides an anatomical, developmental linkage between the cranial vault and formation of

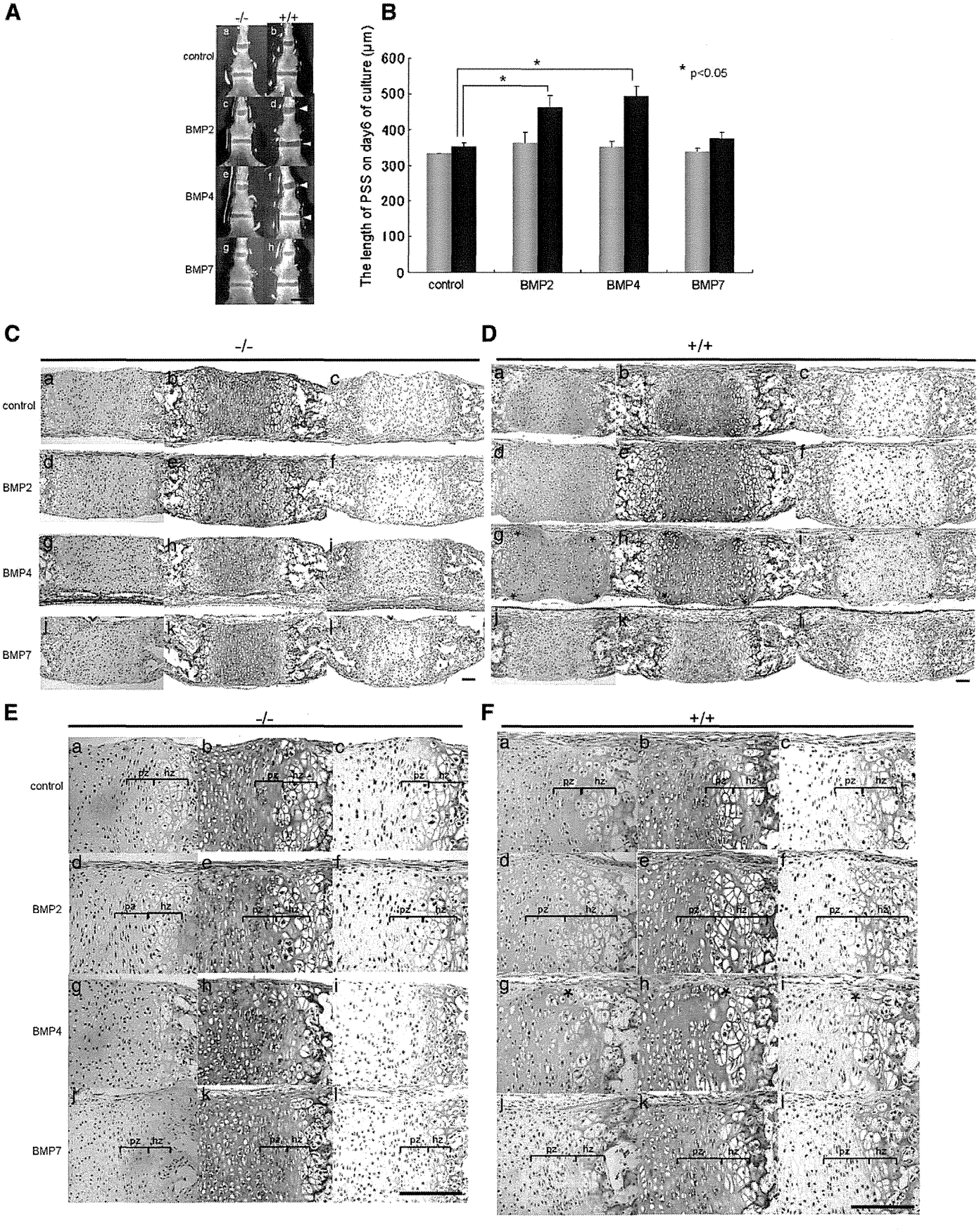

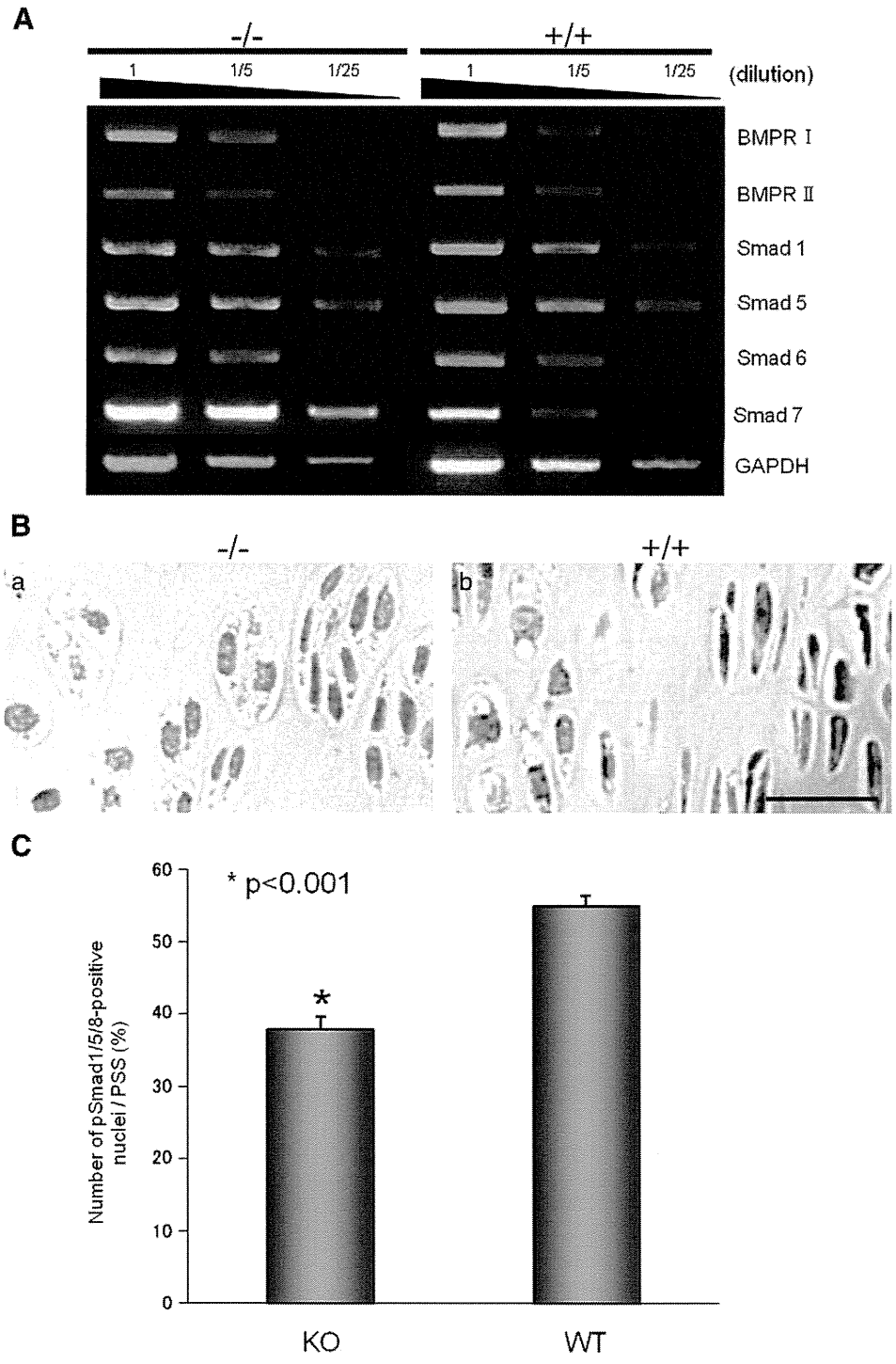

Fig. 6. Id2 regulates BMP signaling in synchondrosis of the cranial base through inhibiting Smad7 expression. (A) Semi-quantitative RT-PCR analysis of BMPRI BMPRII Smad1, Smad5, Smad6, and Smad7 expression in cranial base synchondrosis. RNA was purified from the cranial base synchondrosis of 2-week-old Id2 KO and WT mice. RT products were fivefold serially diluted and subjected to PCR. Reduced glyceraldehyde-phosphate dehydrogenase (GAPDH) was used as an internal control. (B) Immunolocalization of phosphorylated Smad 1/5/8 in Id2-deficient (a) and wild-type (b) mice. (C) The number of pSmad 1/5/8 — positive nuclei in PSS per section was counted in transverse sections of Id2-deficient (left bar) as well as wild-type (right bar) mice. Three sections were prepared from three different mice.

the craniofacial skeleton. Moreover, this growth center is relevant to the temporal and positional cues for the growth and development of the maxilla and mandible [32]. In addition to maxillary hypoplasia, retarded hypertrophic differentiation as well as inhibited cell proliferation in both PSS and SOS was found in Id2 KO mice in postnatal week 2 (Figs. 2C, D, G, and H; Figs. 3A and B). The histological and morphological differences between Id2 KO and WT mice were not observed at birth (Figs. 1L and M; Fig. 2A). The severity of maxillary hypoplasia in Id2-deficient mice increased with growth after birth (Fig. 1J). These results demonstrate that postnatal abnormal growth and development of synchondroses in the cranial base result in maxillary hypoplasia. Previous studies using KO mice identified several genes that regulated embryonic and postnatal growth of the cranial base. As an example, a genetic ablation of the latent TGF-β-binding protein (*Ltbp-3*) contributed to the obliteration of cranial base synchondrosis and a dome-shaped skull [36]. Premature

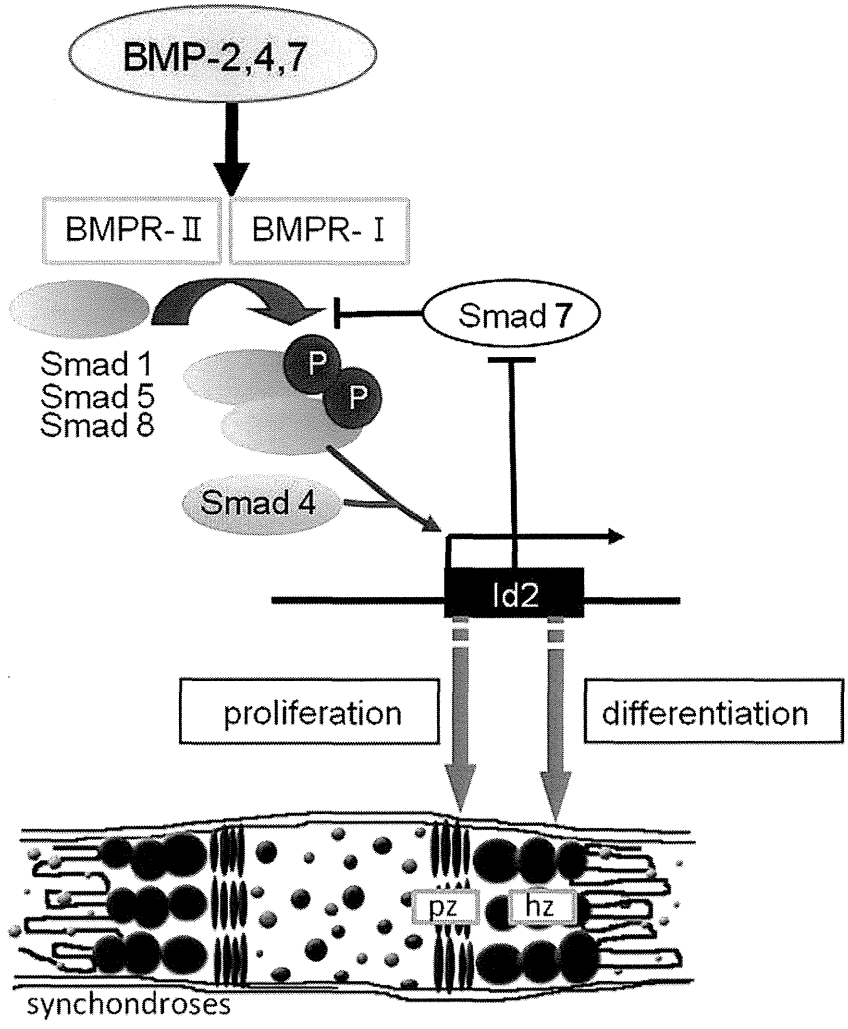

Fig. 7. Diagrammatic representation of the function of Id2 acting downstream of BMP signaling through inhibiting Smad7 in cranial base synchondroses during the postnatal growth period. Inhibition of Smad7 function by Id2 proteins. In general, Smad7, one of the inhibitory Smads, interferes with the recruitment and phosphorylation of R-Smads. Id2 inhibits the functions of Smad7. Id2 exists in proliferating and hypertrophic chondrocytes at the synchondrosis of the cranial base. Id2 acts on receptors on hypertrophic chondrocytes to keep them hypertrophic and, thereby, promotes the production of BMP2 and BMP4 through Smad. Id2 acts on receptors on proliferating chondrocytes to keep them proliferating and, thereby, promotes the production of BMP7 through Smad.

hypertrophy of the synchondrosis was found in *Ltbp-3* knockout mice [36]. A premature closure of the cranial base PSS, as well as SOS and accompanying craniofacial malformation, was observed in the conditional KO mouse strains of polycystin-1 (*Pkd-1*) [12]. Even though these studies did not report whether or not the mutant mice sustained jaw deformities, their results clearly demonstrated a link between craniofacial deformity and impaired synchondroses of the cranial base. Furthermore, cranial malformation of these mutant mice seemed to appear before birth, since the abnormality of synchondroses has been observed during embryonic development.

Studies have reported that the chondrogenic potential of cells derived from developing mouse craniofacial tissues was regulated via the alteration of Id protein functions through over-expression of the bHLH factor [37]. Mouse trunk neural crest cells, which do not contribute skeletal derivatives, can undergo chondrogenesis and the expression of Id2 is up-regulating by FGF2 treatment in vitro [38]. Proper expression of Id2 is important to chondrogenic differentiation of ATDC cells [39]. It was reported that Id2 was expressed in proliferating chondrocytes of growth plate at E16.5 mouse embryo by immunohistochemistry [39]. Furthermore, the expression of Id2 was showed in proliferating chondrocytes of the developing digits in chick embryo, and expression of Id2 in vivo and in vitro was up-regulated by BMP7 supplement [40]. Indeed, we also detect the Id2 expression in proliferating chondrocytes of the synchondrosis of the cranial base at postnatal developing stage (Fig. 4B). Although these results suggest that Id2 are critical controls for chondrogenesis and osteogenesis in vitro systems and are expressed in chondrocytes in vivo, the physiological function for Ids has not been demonstrated. Our report is the first to demonstrate the involvement of the Id2 gene in chondrocyte differentiation, chondrocyte proliferation, and endochondral ossification in vivo. The Id2 knock-out mouse model showed the inhibition of cell proliferation and hypertrophic differentiation of chondrocytes in the cranial base synchondrosis. This mouse model provides a unique opportunity to explain the physiological activity of Id2 transcriptional controls and its role in postnatal jaw deformities.

Inhibitory Smads including Smad6 and Smad7 inhibit the phosphorylation of receptor-regulated Smads (R-Smad) [41]. Smad6 inhibits BMP signaling, whereas Smad7 inhibits both TGF-β and BMP signaling [42]. Smad7 is expressed in growth plate cartilage [43]. In vitro studies using cell culture systems or the organ culture of mandibular explants have shown that Smad7 inhibits chondrocyte differentiation and/or proliferation induced by TGF-β [44,45] and BMP [46,47]. These in vitro studies demonstrated the down-regulation of R-Smad activation by Smad7 in chondrocytes. Recently, Smad7 was found to inhibit chondrocyte differentiation at multiple steps during

endochondral bone formation using conditional transgenic mice [48]. Furthermore, BMP-induced cartilaginous nodule formation was down-regulated by the overexpression of Smad7, but not Smad6 [48]. Indeed, in our experiment, the up-regulation of Smad7 as a result of Id2 abrogation led to the inhibition of chondrocyte proliferation and differentiation.

In summary, the present study demonstrated that Id2 functions by acting downstream of BMP signaling to regulate cartilage formation during postnatal growth and development by enhancing BMP signals through inhibiting Smad7 expression. These interactions contribute to endochondral ossification in the cranial base synchondrosis during the growth period.

Supplementary materials related to this article can be found online at doi:10.1016/j.bone.2011.09.049.

Acknowledgments

This study was supported by a Grant-in-Aid for Young Scientists (B) from the Japanese Society for the Promotion of Science. We thank the all members of Translation Research Center (Kyoto University Hospital) for the great technical support and discussions in this study.

References

[1] Proffit William R, White Raymond P, Sarver Jr David M, editors. Contemporary treatment of dentofacial deformity. Philadelphia, USA: Mosby; 2003.
[2] Susami R, Asai Y, Hirose K, Hosoi T, Hayashi I. Prevalence of malocclusion in Japanese school children. 4. The frequency of mandibular overjet. Nippon Kyosei Shika Gakkai Zasshi 1972;31:319–24.
[3] Tang EL. The prevalence of malocclusion amongst Hong Kong male dental students. Br J Orthod 1994;21:57–63.
[4] Allwright WC, Bundred WH. A survey of handicapping dentofacial anomalies among Chinese in Hong Kong. Int Dent J 1964;14:505–19.
[5] Emirich RE, Brodie AG, Blayney JR. Prevalence of class I, class II, class III malocclusions (Angle) in an urban population; an epidemiological study. J Dent Res 1965;44: 947–53.
[6] Xue F, Wong RW, Rabie AB. Genes, genetics, and Class III malocclusion. Orthod Craniofac Res 2010;13:69–74.
[7] Singh GD. Morphologic determinants in the etiology of class III malocclusions: a review. Clin Anat 1999;12:382–405.
[8] Li Q, Zhang F, Li X, Chen F. Genome scan for locus involved in mandibular prognathism in pedigrees from China. PLoS One 2010;5.
[9] Cruz RM, Krieger H, Ferreira R, Mah J, Hartsfield Jr J, Oliveira S. Major gene and multifactorial inheritance of mandibular prognathism. Am J Med Genet A 2008;146A:71–7.
[10] Yamaguchi T, Park SB, Narita A, Maki K, Inoue I. Genome-wide linkage analysis of mandibular prognathism in Korean and Japanese patients. J Dent Res 2005;84:255–9.
[11] Ranly DM. Craniofacial growth. Dent Clin North Am 2000;44:457–70.
[12] Kolpakova-Hart E, McBratney-Owen B, Hou B, Fukai N, Nicolae C, Zhou J, et al. Growth of cranial synchondroses and sutures requires polycystin-1. Dev Biol 2008;321:407–19.
[13] Sugai M, Gonda H, Nambu Y, Yokota Y, Shimizu A. Role of Id proteins in B lymphocyte activation: new insights from knockout mouse studies. J Mol Med 2004;82: 592–9.
[14] Yokota Y, Mansouri A, Mori S, Sugawara S, Adachi S, Nishikawa S, et al. Development of peripheral lymphoid organs and natural killer cells depends on the helix–loop–helix inhibitor Id2. Nature 1999;397:702–6.
[15] Sugai M, Gonda H, Kusunoki T, Katakai T, Yokota Y, Shimizu A. Essential role of Id2 in negative regulation of IgE class switching. Nat Immunol 2003;4:25–30.
[16] Norton JD. ID helix–loop–helix proteins in cell growth, differentiation and tumorigenesis. J Cell Sci 2000;113:3897–905.
[17] Iavarone A, Garg P, Lasorella A, Hsu J, Israel MA. The helix–loop–helix protein Id-2 enhances cell proliferation and binds to the retinoblastoma protein. Genes Dev 1994;8:1270–84.
[18] Atherton GT, Travers H, Deed R, Norton JD. Regulation of cell differentiation in C2C12 myoblasts by the Id3 helix–loop–helix protein. Cell Growth Differ 1996;7:1059–66.
[19] Lyden D, Young AZ, Zagzag D, Yan W, Gerald W, O'Reilly R, et al. Id1 and Id3 are required for neurogenesis, angiogenesis and vascularization of tumour xenografts. Nature 1999;401:670–7.
[20] Ying QL, Nichols J, Chambers I, Smith A. BMP induction of Id proteins suppresses differentiation and sustains embryonic stem cell self-renewal in collaboration with STAT3. Cell 2003;115:281–92.
[21] Abe J. Bone morphogenetic protein (BMP) family, SMAD signaling and Id helix–loop–helix proteins in the vasculature: the continuous mystery of BMPs pleotropic effects. J Mol Cell Cardiol 2006;41:4–7.
[22] Hoffmann A, Gross G. BMP signaling pathways in cartilage and bone formation. Crit Rev Eukaryot Gene Expr 2001;11:23–45.
[23] Takahashi K, Nuckolls GH, Tanaka O, Semba I, Takahashi I, Dashner R, et al. Adenovirus-mediated ectopic expression of Msx2 in even-numbered rhombomeres induces apoptotic elimination of cranial neural crest cells in ovo. Development 1998;125:1627–35.
[24] Mukhopadhyay P, Singh S, Greene RM, Pisano MM. Molecular fingerprinting of BMP2- and BMP4-treated embryonic maxillary mesenchymal cells. Orthod Craniofac Res 2006;9:93–110.
[25] Mukhopadhyay P, Webb CL, Warner DR, Greene RM, Pisano MM. BMP signaling dynamics in embryonic orofacial tissue. J Cell Physiol 2008;216:771–9.
[26] Hollnagel A, Oehlmann V, Heymer J, Rüther U, Nordheim A. Id genes are direct targets of bone morphogenetic protein induction in embryonic stem cells. J Biol Chem 1999;274:19838–45.
[27] Korchynskyi O, ten Dijke P. Identification and functional characterization of distinct critically important bone morphogenetic protein-specific response elements in the Id1 promoter. J Biol Chem 2002;277:4883–91.
[28] López-Rovira T, Chalaux E, Massagué J, Rosa JL, Ventura F. Direct binding of Smad1 and Smad4 to two distinct motifs mediates bone morphogenetic protein-specific transcriptional activation of Id1 gene. J Biol Chem 2002;277:3176–85.
[29] Arron JR, Winslow MM, Polleri A, Chang CP, Wu H, Gao X, et al. NFAT dysregulation by increased dosage of DSCR1 and DYRK1A on chromosome 21. Nature 2006;441:595–600.
[30] Murashima-Suginami A, Takahashi K, Kawabata T, Sakata T, Tsukamoto H, Sugai M, et al. Rudiment incisors survive and erupt as supernumerary teeth as a result of USAG-1 abrogation. Biochem Biophys Res Commun 2007;359:549–55.
[31] Murashima-Suginami A, Takahashi K, Sakata T, Tsukamoto H, Sugai M, Yanagita M, et al. Enhanced BMP signaling results in supernumerary tooth formation in USAG-1 deficient mouse. Biochem Biophys Res Commun 2008;369:1012–6.
[32] Bjork A. Cranial base development. Am J Orthod 1995;41:198–225.
[33] Lei WY, Wong RW, Rabie AB. Factors regulating endochondral ossification in the spheno-occipital synchondrosis. Angle Orthod 2008;78:215–20.
[34] Wolff G, Wienker TF, Sander H. On the genetics of mandibular prognathism: analysis of large European noble families. J Med Genet 1993;30:112–6.
[35] Frazier-Bowers S, Rincon-Rodriguez R, Zhou J, Alexander K, Lange E. Evidence of linkage in a Hispanic cohort with a Class III dentofacial phenotype. J Dent Res 2009;88:56–60.
[36] Dabovic B, Chen Y, Colarossi C, Obata H, Zambuto L, Perle MA, et al. Bone abnormalities in latent TGF-[beta] binding protein (Ltbp)-3-null mice indicate a role for Ltbp-3 in modulating TGF-[beta] bioavailability. J Cell Biol 2002;156:227–32.
[37] Mukhopadhyay P, Rezzoug F, Webb CL, Pisano MM, Greene RM. Suppression of chondrogenesis by Id helix–loop–helix proteins in murine embryonic orofacial tissue. Differentiation 2009;77:462–72.
[38] Ido A, Ito K. Expression of chondrogenic potential of mouse trunk neural crest cells by FGF2 treatment. Dev Dyn 2006;235:361–7.
[39] Yang L, Ma X, Lyone A, Zou J, Blackburn ML, Pan J, et al. Proper expression of helix–loop–helix protein Id2 is important to chondrogenic differentiation of ATDC5 cells. Biochem J 2009;419:635–43.
[40] Lorda-Diez CI, Torre-Pérez N, García-Porrero JA, Hurle JM, Montero JA. Expression of Id2 in the developing limb is associated with zones of active BMP signaling and marks the regions of growth and differentiation of the developing digits. Int J Dev Biol 2009;53:1495–502.
[41] Massagué J, Seoane J, Wotton D. Smad transcription factors. Genes Dev 2005;19: 2783–810.
[42] Goto K, Kamiya Y, Imamura T, Miyazono K, Miyazawa K. Selective inhibitory effects of Smad6 on bone morphogenetic protein type I receptors. J Biol Chem 2007;282:20603–11.
[43] Sakou T, Onishi T, Yamamoto T, Nagamine T, Sampath T, Ten Dijke P. Localization of Smads, the TGF-beta family intracellular signaling components during endochondral ossification. J Bone Miner Res 1999;14:1145–52.
[44] Ito Y, Bringas Jr P, Mogharei A, Zhao J, Deng C, Chai Y. Receptor-regulated and inhibitory Smads are critical in regulating transforming growth factor beta-mediated Meckel's cartilage development. Dev Dyn 2002;224:69–78.
[45] Scharstuhl A, Diepens R, Lensen J, Vitters E, van Beuningen H, van der Kraan P, et al. Adenoviral overexpression of Smad-7 and Smad-6 differentially regulates TGF-beta-mediated chondrocyte proliferation and proteoglycan synthesis. Osteoarthritis Cartilage 2003;11:773–82.
[46] Fujii M, Takeda K, Imamura T, Aoki H, Sampath TK, Enomoto S, et al. Roles of bone morphogenetic protein type I receptors and Smad proteins in osteoblast and chondroblast differentiation. Mol Biol Cell 1999;10:3801–13.
[47] Valcourt U, Gouttenoire J, Moustakas A, Herbage D, Mallein-Gerin F. Functions of transforming growth factor-beta family type I receptors and Smad proteins in the hypertrophic maturation and osteoblastic differentiation of chondrocytes. J Biol Chem 2002;277:33545–58.
[48] Iwai T, Murai J, Yoshikawa H, Tsumaki N. Smad7 Inhibits chondrocyte differentiation at multiple steps during endochondral bone formation and down-regulates p38 MAPK pathways. J Biol Chem 2008;283:27154–64.

SCIENTIFIC REPORTS

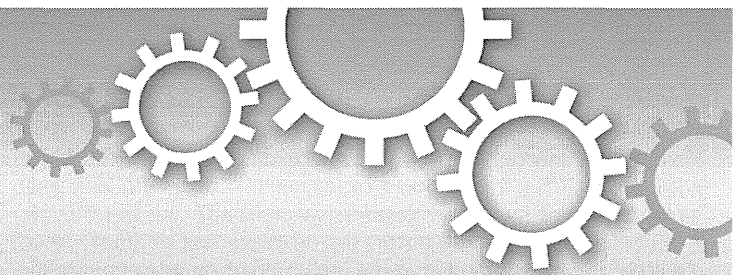

OPEN

SUBJECT AREAS:
DEVELOPMENT
AUTOIMMUNITY
DIFFERENTIATION
IMMUNOGENETICS

Received
26 June 2012

Accepted
23 August 2012

Published
7 September 2012

Correspondence and requests for materials should be addressed to M.S. (msugai@virus.kyoto-u.ac.jp)

* Current address: Bioprocessing Technology Institute, A*STAR 20 Biopolis Way #06-01 Centros Singapore 138668.

In situ differentiation of CD8αα T cells from CD4 T cells in peripheral lymphoid tissues

Yukiko Nambu[1]*, Tatsunari Hayashi[1], Kyoung-Jin Jang[1], Koji Aoki[2], Hiroto Mano[1], Keiko Nakano[1], Motomi Osato[3,4], Katsu Takahashi[5], Katsuhiko Itoh[6], Satoshi Teramukai[7], Toshihisa Komori[8], Jun Fujita[6], Yoshiaki Ito[3,4], Akira Shimizu[1] & Manabu Sugai[1]

[1]Department of Experimental Therapeutics, Translational Research Center, Kyoto University Hospital, 54 Shogoin-Kawahara-cho, Sakyo-ku, Kyoto 606-8507, Japan, [2]Tenure-Track Program for Innovative Research, University of Fukui, 23-3 Matsuokashimoaizuki, Eiheiji-cho, Yoshida-gun, Fukui, Japan. 910-1193, [3]Cancer Science Institute of Singapore, National University of Singapore, 14 Medical Drive, Singapore 117599, Singapore, [4]Institute of Molecular and Cell Biology, 61 Biopolis Drive, Proteos, Singapore 138673, Singapore, [5]Department of Oral and Maxillofacial Surgery, Graduate School of Medicine, Kyoto University, 54 Shogoin-Kawahara-cho, Sakyo-ku, Kyoto 606-8507, Japan, [6]Department of Clinical Molecular Biology, Graduate School of Medicine, Kyoto University, 54 Shogoin-Kawahara-cho, Sakyo-ku, Kyoto 606-8507, Japan, [7]Department of Clinical Trial Design and Management, Translational Research Center, Kyoto University Hospital, 54 Shogoin-Kawahara-cho, Sakyo-ku, Kyoto 606-8507, Japan, [8]Department of Cell Biology, Unit of Basic Medical Sciences, Nagasaki University Graduate School of Biomedical Sciences, Nagasaki 852-8588, Japan.

Mutually exclusive cell fate determination of CD4 helper or CD8 killer T cells occurs in the thymus. These T-cell subsets are not believed to redirect other lineages. Here we showed that retinoic acid and transforming growth factor-β1 promoted the differentiation of CD8αα T cells from CD4 T cells in a Runx3-dependent manner. These cells were inferred to belong to immunoregulatory populations because subpopulations of CD8αα+TCRαβ T cells are known to suppress activated T cells, and mice with Runx3$^{-/-}$ T cells showed defects during recovery from experimental allergic encephalomyelitis. Our results demonstrate that CD4 T cells play fundamental roles in controlling immune reactions through promotion and attenuation. We accordingly anticipate that clarifying the mechanisms underlying this process will provide insights leading to autoimmune and immunodeficiency disease therapies.

During T cell maturation, T-cell receptor (TCR) αβ-bearing cells express both CD4 and CD8 (double-positive thymocytes) molecules on their surface. Transition from double to single positive (CD4+CD8− or CD4−CD8+) requires the selection of TCRαβ with intrathymic ligands that are presented by major histocompatibility complexes (MHCs). CD4 and CD8 coreceptors interact with MHC class II and I molecules, respectively, thereby resulting in the interaction of TCRαβ with ligands/MHC complexes and stabilizing CD4 or CD8 expression on maturing TCRαβ T cells. Simultaneously, thymocytes diverge into functionally distinct CD4 helper and CD8 killer cells[1]. A correlation between the mechanisms of antigen recognition and functional divergence of T cells suggests that the commitment of these cells is irreversible. The redirection of CD4 T cells to the CD8 lineage and vice versa is not believed to occur in the periphery.

Establishment of central and peripheral tolerance is important for maintaining immunological homeostasis. In addition to naturally occurring CD4+CD25+Foxp3+ regulatory T cells (nTregs), several phenotypically and functionally distinct regulatory T-cell populations have been suggested[2–6]. To date, at least four CD8+ Treg subsets have been identified, and these include CD8+CD28−, CD8+CD25+, CD8+CD122+, and CD8αα T cells. Among them, two CD8+ T-cell subsets exhibit a special property in suppressing activated, but not naïve, T cells[7–9]. CD8αβ+CD122+CD44+ inducible costimulator ligand (ICOSL)+ TCR αβ+ T cells attenuate immune responses by inhibiting follicular T helper cell (T_{FH}) via recognition of Qa-1, which is expressed on T_{FH} cells in an activation-dependent manner[7]. The CD8αα+CD122+TCRαβ+ T-cell subset was identified during the screening of Treg cells that inhibit experimental autoimmune encephalomyelitis (EAE) in mice[10,11]. This CD8αα T-cell subset recognizes the pathogenic TCR-derived peptide that is present on the Qa-1 molecule of pathogenic T cells in an activation-dependent manner and inhibits pathogenic T cells. In addition, an immunoregulatory role of CD8αα+TCRαβ+ T cells has been shown in two other autoimmune disease models. First, transfer of

CD8ααTCRαβ T cells inhibits colitis, induced by the adoptive transfer of naïve CD4 T cells into severe combined immunodeficient (SCID) mice[6]. Second, non-obese diabetic (NOD) mice are defective in the generation of CD8ααTCRαβ T cells, suggesting a regulatory role of these cell populations[12]. In addition, genetic control elements, which are required for clonal deviation to CD8αα T cells, also regulate rescue from clonal deletion of nTregs in the thymus[13], suggesting that these different subsets of immunoregulatory T cells share a common thymic selection mechanism.

The developmental pathway of CD8αα+TCRαβ+ T cells is controversial because of the following findings. First, the accumulation of autoreactive TCRs was observed in the repertoire of CD8αα+TCRαβ+ T cells[14]. Second, CD8αα+TCRαβ+ T cells comprise only a small portion of T cells in the lymph node and spleen (<1% of T cells) but a large portion (approximately 40% of T cells) in the intraepithelium of the gut. For this reason it was previously believed that CD8αα+TCRαβ+ T cells were of extrathymic origin and differentiated locally in the gut; however, they are now considered to originate in the thymus[15]. In the thymus, CD8αα+TCRαβ+ precursor T cells were selected by high-affinity self-antigens, such as nTregs[12,16,17]. The selected precursor T cells were CD4- and CD8-double-negative cells. The final maturation of these cells, including the expression of CD8αα, occurs in the gut[18]. Transforming growth factor (TGF)-β1 plays a key role in the generation of nTregs and CD8αα T cells during selection in the thymus[19,20]. Thus, the regulatory factors that control development of CD8αα+TCRαβ+ intestinal intraepithelial lymphocytes (IELs) and the molecular pathways of this cell population have been elucidated. However, the origin of CD8αα+TCRαβ+ T cells outside intestines and the factors required for their generation are incompletely understood.

In this study, we showed that immune reactions promote the differentiation of CD8αα+TCRαβ+ T cells from naïve CD4 T cells within peripheral lymphoid tissues. Among the factors induced by inflammation, TGF-β1, all-trans retinoic acid (atRA), and interleukin (IL)-2 are indispensable for the differentiation of CD8αα T cells. Striking similarities were observed between induced Tregs (iTregs) and CD8αα T cells, with the same signals required for the differentiation of iTregs. In addition, Runx3-deficient CD4 T cells have lost their ability to become CD8αα T cells, indicating that Runx3 plays a critical role in this differentiation. Furthermore, mice whose T cells were Runx3-deficient showed defects in recovery from EAE. Thus CD8αα Tregs were confirmed to be generated in the thymus and periphery, like CD4+Foxp3+ Tregs, and the signals required for CD8αα Tregs were the same as those required for CD4+Foxp3+ Tregs. We thus demonstrated that the newly identified Treg subset, namely CD8αα Tregs that are derived from CD4 T cells, plays an immunoregulatory role in EAE.

Results

Generation of CD8αα T cells in the spleen by immunization. In addition to CD4+CD25+Foxp3+ T cells[21–23], several populations have been identified as immunoregulatory cells[7,10,24,25]. CD8 Treg subsets negatively regulate activated, but not naïve, T cell functions[7,10,24,25]. Among these cell subsets, CD8ααTCRαβ T cells have been reported to play important roles in the gut mucosal immunity and prevent autoimmune diseases[6,12,13]. However, the origin of this subset and mechanisms of its development remain unclear. The initial commitment of CD8αα T cells occurs in the thymus following exposure to agonist self-peptides[16–18], and their generation requires a TGF-β1 signal[19]. When positively selected CD8αα TCRαβ precursor T cells reach the gut, they express CD8αα molecules in an IL-15-dependent manner[18]. Importantly, the expression of CD8αα is induced on CD8αβ T cells by immunization and is required for the generation of memory CD8αβ T cells[26,27]. We accordingly examined the effect of immunization on the generation of CD8αα single-positive cells in the spleen. As anticipated, immunization induced the generation of CD8αα single-positive T cells (6.5% of CD4−CD8αβ−CD8αα+TCRβ+ T cells within CD4− T cells in immunized spleen compared with 2.5% in non-immunized spleen; Fig. 1A).

Generation of CD8αα T cells from CD4TCRαβ T cells in Rag2$^{-/-}$ mice. With the aim of identifying the subsets that potentially differentiate into CD8αα T cells, their generation was examined at day 20 after naïve CD4 and CD8αβ T cells were adoptively transferred into Rag2$^{-/-}$ mice. Whereas CD8αα T cells were not found in either case after 20 days, in some Rag2$^{-/-}$ mice that received naïve CD4 T cells they were found after approximately 6 months. A few CD8αα-positive cells were found in all tissues examined, with a significantly larger number observed in Peyer's patches (PPs; Fig. 1B). These observations indicate that naïve CD4 T cells can differentiate into CD8αα T cells, at least under these experimental conditions.

TGF-β1, atRA, and IL-2 promote differentiation of CD8ααTCRαβ Tregs from naïve CD4 T cells *in vitro*. To investigate the mechanisms of differentiation from CD4 into CD8αα T cells, we first focused on the factors required for the generation of iTregs or CD4+Foxp3+ cells. We added the factors to a conventional *in vitro* CD4 T-cell differentiation assay. IL-2, TGF-β1, and atRA generated CD8αα T cells from CD4 T cells (Fig. 2A). Although atRA played only a supporting role in the differentiation of iTreg cells, the generation of CD8αα T cells depended on all three factors (Fig. 2A and data not shown). To exclude the possibility that CD8αα T cells were derived from contaminated CD8αβ cells, CD8αβ T cells were cultured under the same conditions as those used for the differentiation of CD8αα from CD4 T cells, and no CD8αα T cells were observed (Fig. 2B). Moreover, CD8αβ T cells have the ability to inhibit CD4-derived CD8αα T cell differentiation, as shown in Fig 2C. These observations indicate that CD4 T cells and not CD8αβ T cells are the major source of peripheral CD8αα T cells. Because ILs play critical roles in the determination of helper T-cell subsets, we further examined the effects of various ILs on the differentiation of CD8αα. Our results showed that IL-2 exerted the strongest effect on the generation of CD8αα T cells (Fig. 2D). Antigen dose has been shown to affect the differentiation of CD8αα T cells. In the thymus, a low concentration of an agonist induces CD8αβ T cells, whereas a high concentration induces CD8αα T cells. atRA concentration influences the differentiation of iTreg and Th17 cells[28,29]. Thus, antigen dose and atRA concentration influence various processes in cell fate determination. We accordingly examined the effects of TCR signal strength and atRA concentration on differentiation of CD8αα T cells. A high percentage of CD8αα T cells was found after culture with strong TCR stimulation and high atRA concentration (Fig. 2E).

Runx3-dependent generation of CD8ααTCRαβ Tregs *in vitro*. With the aim of characteristizing CD8αα T cells (CD8α positive fraction in Fig 3A or CD8αα cells in Fig 3B) that were generated *in vitro*, their gene expression profile was compared with iTregs (CD8 negative fraction shown in Fig 3A or iTreg cells in Fig 3B) derived from the same culture condition (as shown in Fig 3A) and previously well-characterized CD8 TCRαβ Tregs[7,9,24,30]. The expression of granzymes A and B increased in the CD8αα population, whereas that of Foxp3 decreased (Fig. 3A, B). The expression of CD122 and ICOSL on the surface was also specifically induced in CD8αα T cells (Fig. 3A). The expression pattern of these genes was similar to that of other CD8 Treg cells[7,9,24,30]. Recent studies have indicated that Runx3 is a major regulator of CD8αβ T cells, while ThPOK is a major regulator of CD4 T cells[31–33]. We accordingly examined the possibility that these factors were involved in the differentiation from CD4 to CD8αα T cells. Runx1 and ThPOK were expressed specifically in naïve CD4 T cells (Fig. 3B). After the generation of CD8αα

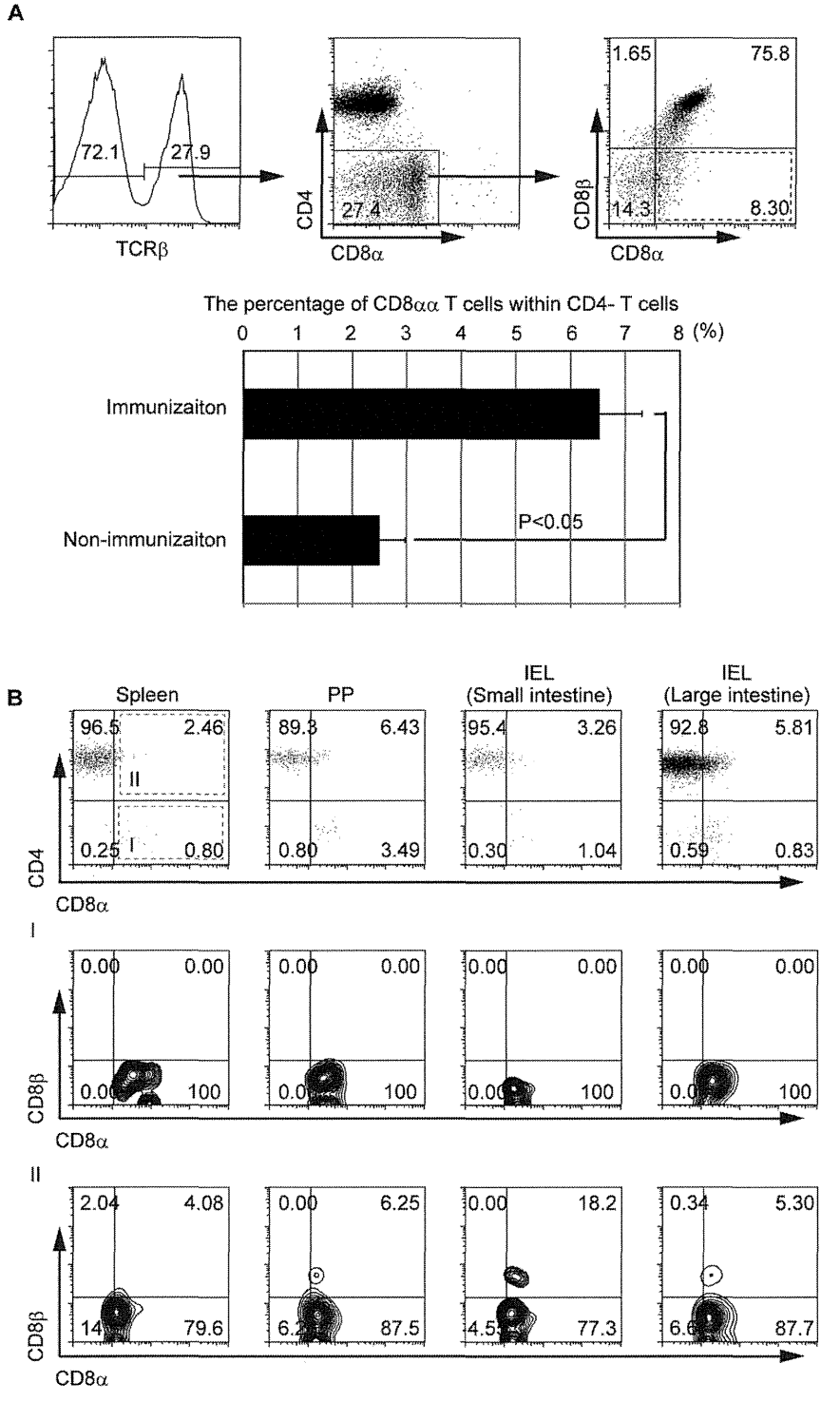

Figure 1 | Generation of CD8αα T cells in Rag2$^{-/-}$ mice. (A) Fluorescence-activated cell sorting (FACS) analysis of CD8αα+CD8αβ−CD4−TCRαβ T cells in the spleen after immunization of WT (C57BL/6) mice with NP-CGG/Alum. Horizontal axis indicate percentage of CD8αα T cells within CD4− T cells. *$p < 0.05$; n = 3. TCR, T-cell receptor. (B) FACS analysis of lymphocytes from Rag2$^{-/-}$ mice (CD45.1) that had received naïve CD4 T cells (CD45.2) 6 months previously. TCRαβ+CD45.2+ cells were examined for CD4 and CD8α expression. CD4−CD8α+ (I) and CD4+CD8α+ (II) T cells were further examined for CD8α and CD8β expression. IELs, intestinal intraepithelial lymphocytes, PP, Peyer's patches. CD8αα T cell differentiations from CD4 T cells in Rag2$^{-/-}$ mice were confirmed in two of four mice analyzed, and representative data are shown.

T cells, only Runx3 expression was observed, while this was not found in the iTreg subset (Fig. 3B). Of note, we had previously found that Runx2 and Runx3 are required for TGF-β1 and atRA signals in IgA class switching in B cells[34,35]. Thus, it was conceivable that Runx3 contributed to the differentiation of CD8αα cells. As anticipated, Runx3$^{-/-}$CD4 T cells were unable to differentiate into CD8αα T cells (Fig. 4). These observations support the hypothesis that CD4-derived CD8αα T cells function as regulatory cells *in vivo* and that Runx3 is essential for the generation of these lineage cells.

Generation of CD8αα Tregs from CD4 T cells *in vivo* requires Runx3. To determine whether CD4 T cells differentiate into CD8αα T cells *in vivo*, naïve CD4 T cells from C57BL/6 (CD45.2)

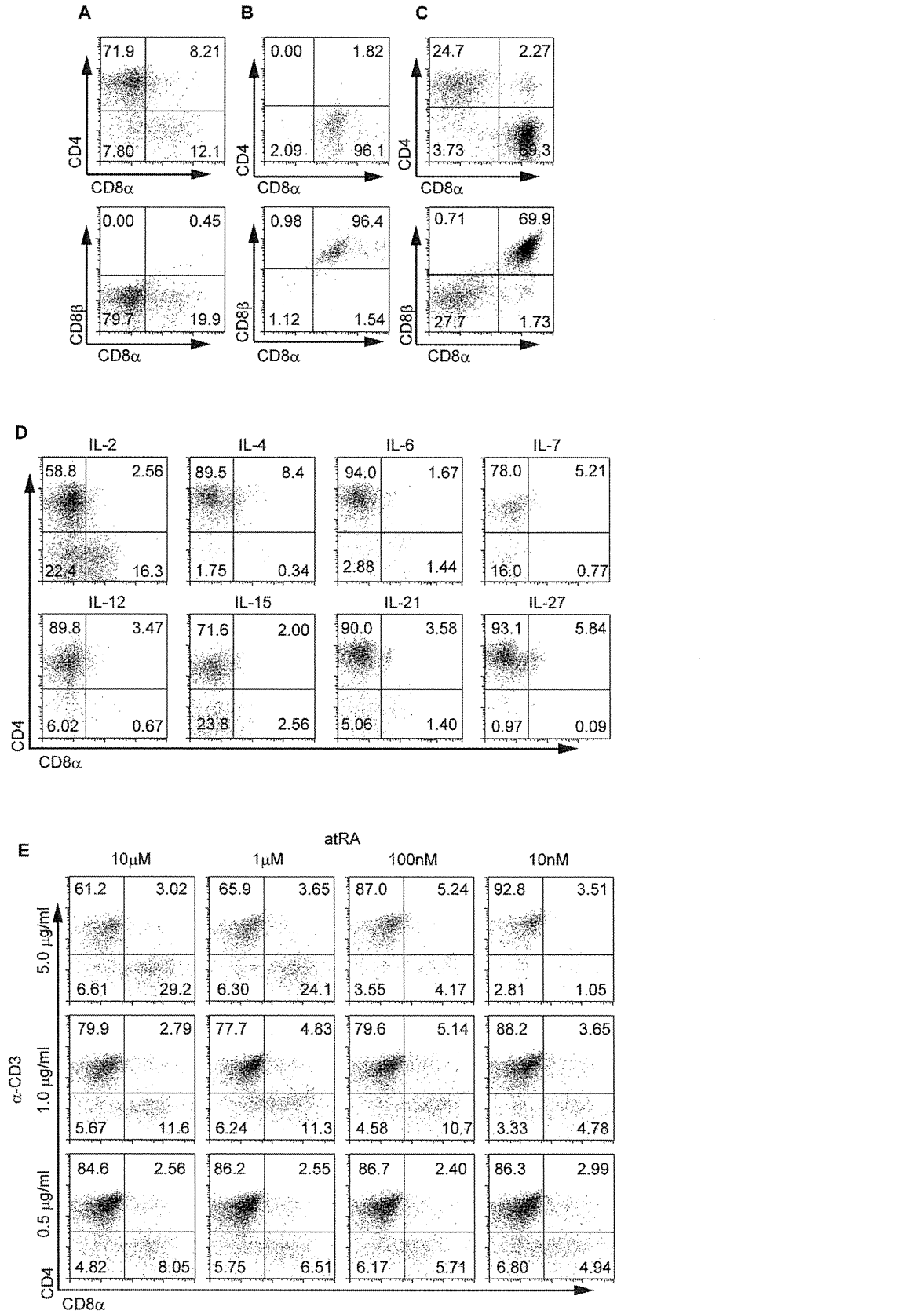

Figure 2 | TGF-β1, atRA, and IL-2 promote differentiation of CD8αα$TCR\alpha\beta$ regulatory T cell (Treg) from naïve CD4 T cells *in vitro*. (A) Naïve CD4+ T cells were stimulated with α-CD28, IL-2, TGF-β1, and atRA on α-CD3ε-coated plates. CD8αα+CD4− T cells were analyzed by FACS. (B) CD8αβ+ T cells were stimulated under conditions mentioned in A. (C) Total spleen T cells (41% CD8αβ+ T cells and 56% CD4 T cells) were stimulated under conditions mentioned in A. (D) Naïve CD4+ T cells were cultured with various ILs and TGF-β1+atRA. (E) Naïve CD4+ T cells were stimulated with TGF-β1, IL-2, and various atRA concentrations on plates coated with indicated concentrations of α-CD3ε. Cell differentiation was analyzed by FACS. All experiments were performed at least thrice; representative data are shown.